Journal of Intelligent & Robotic Systems (2024) 110:9
https://doi.org/10.1007/s10846-023-02016-9

REGULAR PAPER

Position and Attitude Tracking Controllers Using Lyapunov Transformations for Quadrotors

João Madeiras[1] · Carlos Cardeira[1] · Paulo Oliveira[1,2]

Received: 20 March 2023 / Accepted: 2 November 2023 / Published online: 12 January 2024

Abstract
In this paper, a novel feedback control strategy for quadrotor trajectory tracking is designed and experimentally tested with proof of exponential stability, using the Lyapunov transformations theory. The controller is derived from an inner-outer loop control structure, namely by considering the position system coupled through an interconnection term with the attitude system. For the design of the position controller, the considered dynamics are worked on the body frame, which is uncommon in the literature, and its synthesis derives from theories such as Pontryagin's maximum principle, Lyapunov theory, and Linear Quadratic Regulator (LQR), which ensure Input-to-state stability, steady-state optimality, and global exponential stability. The attitude system is based on an error quaternion parameterization via a nonlinear coordinate transformation matrix followed by a state input feedback, rendering the system linear and time-invariant. Under a correct transformation, LQR theory ensures almost exponential stability and steady-state optimality for the overall interconnected closed-loop systems. Experimental and simulation results illustrate the performance of the tracking system onboard a quadrotor.

Keywords Nonlinear control · Interconnected systems · Stability · Quadrotor

1 Introduction

In recent years, research and applications for quadrotors have been on high demand due to its special structure that allows them to vertical take off and landing, as well as hovering. Such capabilities allow quadrotors to perform difficult tasks, e.g. monitoring, surveying, inspection, search and rescue.

To produce viable solutions to cope with these types of tasks, control laws that emphasize robustness and efficiency are of paramount importance. Furthermore, the quadrotor is a highly nonlinear, underactuated vehicle with coupled dynamics, which constrains the controller design and stability analysis. Over the past years, numerous controllers have been proposed [1]. In [2], linear control techniques, such as the linear quadratic regulator (LQR) were successfully implemented for low-speed indoor flights. Although the linear techniques are successful, most of the times their reliance on linearization of the quadcopter dynamics restricts their ability to fully explore the vehicle's flight envelope and establish an explicit region of attraction for stability. In the literature, a miscellany of nonlinear approaches can be found, such as feedback linearization [3], backstepping [4], differential flatness [5], and sliding-mode control (SMC).

The majority of existing works adopt the inner-outer loop methodology or backstepping techniques to address the interconnection term that arises from the underactuation of quadrotors. For example, in [6, 7], a geometric control approach is employed on the special Euclidean group SE(3) to mitigate singularities and complexities associated with local coordinates. The desired attitude is formulated to align the total thrust direction with the required thrust for tracking a specified position command. Subsequently, the control moment is designed to accurately adjust and track the desired attitude. The authors in [5] address the challenges of designing smooth and feasible trajectories, considering the underactuated nature of quadrotors and control

✉ João Madeiras
joao.madeiras@tecnico.ulisboa.pt

✉ Carlos Cardeira
carlos.cardeira@tecnico.ulisboa.pt

✉ Paulo Oliveira
paulo.j.oliveira@tecnico.ulisboa.pt

[1] IDMEC - Institute of Mechanical Engineering, Instituto Superior Técnico, Universidade de Lisboa, Lisboa 1049-001, Portugal

[2] ISR - Institute for Systems and Robotics, Instituto Superior Técnico, Universidade de Lisboa, Lisboa 1049-001, Portugal

input constraints. The paper explores mathematical modeling, optimization algorithms, and control strategies to generate minimum snap trajectories and enable precise tracking by quadrotors. The authors in [8], tackle the problem of vectored-thrust UAVs using an inner-loop paradigm and integral Input-to-state stability (ISS) techniques to analyze the resulting pseudo cascade structure. The proposed strategy exhibits superior performance compared to other strategies with a similar basin of attraction. Recent significant contributions to quadrotor control, which combine hierarchical control with geometric feedback, can be found in [9, 10], and [11]. The Backstepping method has been applied in several studies, as referenced in [12, 13], and [14], to control underactuated quadrotors. In these approaches, the attitude error is derived either from the error in the thrust direction or through the use of traditional backstepping techniques. Consequently, the interconnection term is skillfully backstepped into the attitude control law, effectively canceling its influence.

The proposed strategy offers a tracking control structure with almost global exponential stability resorting to the nonlinear system of a quadrotor in the sensor space and error domain. The solution blends linear methods, nonlinear transformations and input-to-stable stability to render the vehicle closed-loop nonlinear systems stable. The controller, designed in the body frame, assumes an hierarchical approach. The position controller is designed through the Maximum Principle followed by a Lyapunov Transformation that renders a nonlinear Riccati equation linear time-invariant (LTI), removing the necessity of solving the Riccati equation over time. The procedure not only guarantees global exponential stability but also minimizes a regular LQR cost function for the position controller. The attitude controller, based on quaternion parameters and the angular velocity relationship, is designed through a nonlinear transformation of coordinates followed by state-input feedback that renders the orientation system LTI. The method ensures almost global stability and a sense of steady-state optimality of the controller.

Moreover, to enhance robustness against unknown disturbances, integrative action is incorporated to both position and attitude errors. Various simulation tests are conducted to evaluate the controller's performance under conditions of moment of inertia variations and when subjected to a pendulum load. Additionally, a trajectory tracking experiment is carried out in an indoor lab to demonstrate the effectiveness of the onboard quadrotor tracking system.

The presented solution proposes a straightforward approach to quadrotor trajectory tracking by employing exact Lyapunov transformations to propagate the properties of linear systems to the nonlinear error dynamics of the vehicle, emphasizing robustness through integrative action and optimality considerations. The proposed methodology incorporates rigid-body translational dynamics expressed in body-fixed coordinates. This has several advantages. For instance, it avoids the algebraic transformation of sensor data to inertial coordinates, which helps mitigate the amplification of noise and biases on attitude estimates. This aligns with the findings of [15], highlighting the undesirability of such transformations. In addition, the use of the body frame, which closely resembles the camera frame in image-based visual servoing, allows for direct application of the proposed method to visual servoing tasks [16]. Furthermore, working with the position dynamics on the body frame enables direct exploitation of accelerometer measurements for body acceleration estimation, enabling the system to effectively cope with certain unmodeled dynamics. This holds true not only for control purposes but also for estimation [17].

This paper is organized as follows. Section 2 introduces the dynamics and kinematics of the quadrotor. The problem statement and control objective are also provided. Section 3 provides the design of an steady-state optimal position control law to guaranteed asymptotic convergence of the closed-loop error to zero. The attitude controller design is also given with stability proof. In Section 4, a comprehensive analysis of stability for the trajectory tracking system is performed. Section 5 shows the simulation and experimental results of the controller, a brief explanation on the gain tuning, and a performance analysis. Concluding remarks are pointed out in Section 6.

Notation

Throughout the paper, bold lower-case letters (e.g. $\boldsymbol{x}$, $\boldsymbol{b}$) denote column vectors, bold upper-case letters (e.g. $\boldsymbol{X}$, $\boldsymbol{K}$) denote matrices, the symbol $\mathbf{0}$ denotes a matrix of zeros and $\boldsymbol{I}$ an identity matrix, both with appropriate dimensions. The i-th element of vector $\boldsymbol{x}$ is denoted by $\boldsymbol{x}_i$. The vectors $\boldsymbol{e}_1$, $\boldsymbol{e}_2$, and $\boldsymbol{e}_3$ denote the unit vectors codirectional with the x, y, and z axes, respectively. The time derivative of $\boldsymbol{s}$ is denoted by $\dot{\boldsymbol{s}}$. The Euclidean norm of vectors is denoted as $\|\boldsymbol{x}\|, \boldsymbol{x} \in \mathbb{R}^n$. In $\mathbb{R}^3$, the skew-symmetric matrix of a generic vector $\boldsymbol{a} \in \mathbb{R}^3$ is defined as $[\boldsymbol{a}\times]$ and given by

$$[\boldsymbol{a}\times] = \begin{bmatrix} 0 & -a_z & a_y \\ a_z & 0 & -a_x \\ -a_y & a_x & 0 \end{bmatrix}.$$

${}^{E}\boldsymbol{s}$ is the vector $\boldsymbol{s}$ expressed in coordinate frame $\{E\}$, and ${}^{B}_{I}\boldsymbol{R}$ is a rotational matrix from the inertial frame $\{I\}$ to the body frame $\{B\}$. Finally, the transpose operator is denoted by the superscript $(\cdot)^T$.

2 Problem Formulation

2.1 Quadrotor Dynamics and Kinematics

Consider the quadrotor vehicle model presented in Fig. 1. The system is equipped with four identical motors and propellers distributed symmetrically, which generate a thrust and torque normal to the plane formed by the rotors. Consider the system body-fixed frame is located at the center of mass of the vehicle. The differential equations that rules the kinematics and dynamics for this specific vehicle can be defined as follows

$$\dot{\boldsymbol{p}} = \boldsymbol{R}\boldsymbol{v} \tag{1}$$

$$\dot{\boldsymbol{v}} = -[\boldsymbol{\omega}\times]\boldsymbol{v} - \frac{T}{m}\boldsymbol{e_3} + \boldsymbol{R}^T g\boldsymbol{e_3} \tag{2}$$

$$\dot{\boldsymbol{q}} = \frac{1}{2}\boldsymbol{\Omega}(\boldsymbol{\omega})\boldsymbol{q} \tag{3}$$

$$\dot{\boldsymbol{\omega}} = -\boldsymbol{J}^{-1}[\boldsymbol{\omega}\times]\boldsymbol{J}\boldsymbol{\omega} + \boldsymbol{J}^{-1}\boldsymbol{\tau} \tag{4}$$

where $m \in \mathbb{R}$ the total mass
$\boldsymbol{J} \in \mathbb{R}^{3\times3}$ the inertia matrix with respect to $\{B\}$
$\boldsymbol{R} \in \mathrm{SO}(3)$ the rotation matrix from $\{B\}$ to $\{I\}$ and follows the Tait-Bryan sequence of rotation Z-Y-X
$\boldsymbol{q} \in \mathbb{R}^4$ the quaternion vector, where $\boldsymbol{q} = \begin{bmatrix}\boldsymbol{q_v}^T & q_4\end{bmatrix}^T$
$\boldsymbol{\omega} \in \mathbb{R}^3$ the angular velocity in $\{B\}$
$\boldsymbol{p} \in \mathbb{R}^3$ the location of the center of mass in $\{I\}$
$\boldsymbol{v} \in \mathbb{R}^3$ the velocity of the center of mass in $\{B\}$, i.e. ${}^B\boldsymbol{v}$
$\boldsymbol{\tau} \in \mathbb{R}^3$ the torque generated by the propeller about the $-\boldsymbol{e}_3$ axis
$T \in \mathbb{R}_{>0}$ the total thrust
and $\boldsymbol{\Omega}(\boldsymbol{\omega}) = \begin{bmatrix} -[\boldsymbol{\omega}\times] & \boldsymbol{\omega} \\ -\boldsymbol{\omega}^{\mathrm{T}} & 0 \end{bmatrix}$.

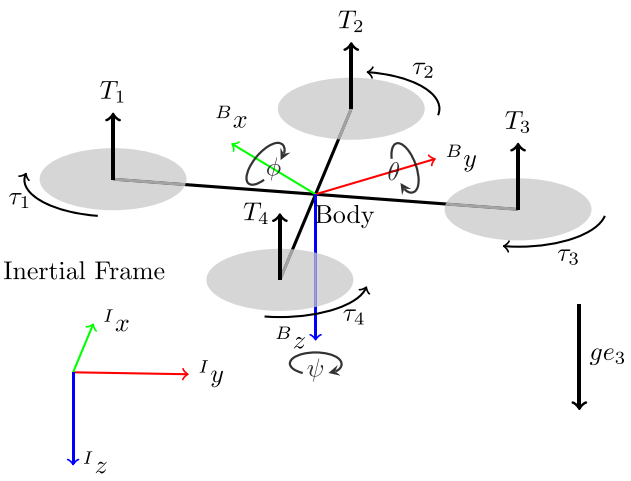

Fig. 1 Quadrotor model

2.2 Problem Formulation

Consider a vehicle with motion equations given by Eqs. 1 to 4. Derive a trajectory tracking control law to follow a prescribed trajectory $\boldsymbol{p}_d(t) \in C^4$ of the location of the center of mass, and a specified heading angle $\psi_d(t) \in C^2$, respecting a balance between performance and energy expenditure. Particularly, the reference derivatives $\dot{\boldsymbol{p}}_d(t)$, $\ddot{\boldsymbol{p}}_d(t)$, $\dddot{\boldsymbol{p}}_d(t)$, $\boldsymbol{p}_d^{(4)}(t)$, $\dot{\psi}_d(t)$ and $\ddot{\psi}_d(t)$ are required to be bounded functions of time. Additionally, assume that a sensor set provides real-time measures of $\boldsymbol{p}$, $\boldsymbol{v}$, $\dot{\boldsymbol{v}}$, $\boldsymbol{q}$, $\boldsymbol{\omega}$ and $\dot{\boldsymbol{\omega}}$. Since the control law is designed in the body frame, the body velocity $\boldsymbol{v}$ can be directly retrieved from an onboard optical flow system, and the body acceleration $\dot{\boldsymbol{v}}$ from the accelerometer. The remaining variables, such as position, angular velocity and quaternion angle, could be accessed from a GPS sensor, a gyroscope, and a sensor fusion with all the above, respectively. The angular acceleration can be estimated through sensor fusion.

In order to guarantee a well-posed control law, the following assumption is established.

Assumption 1 The angular velocity $\boldsymbol{\omega}$ and angular acceleration $\dot{\boldsymbol{\omega}}$ of the vehicle are bounded signals.

From a practical point of view, Assumption 1 is not limitative since the systems presented herein are in fact finite energy systems that ensemble achievable physical vehicles and sensors.

3 Controller Design

In furtherance of tackling the problem stated in Section 2.2, a nonlinear hierarchical control law is proposed. The position and attitude systems are addressed separately. Pontryagin's principle and LQR theory aligned with Lyapunov theory are applied to stabilize the vehicle. Through a set of particular Lyapunov nonlinear transformations, the vehicle dynamics becomes linear, enabling the exploitation of linear techniques, hence, a straightforward procedure to tune the controller. The schematic of the controller is depicted in Fig. 2.

3.1 Position Tracking Control

Suppose that the desired position of the quadrotor represented in inertial frame is $\boldsymbol{p}_d = \begin{bmatrix}x_d & y_d & z_d\end{bmatrix}^T$. The position error is defined as

$$\boldsymbol{e_p} = \boldsymbol{p} - \boldsymbol{p}_d, \tag{5}$$

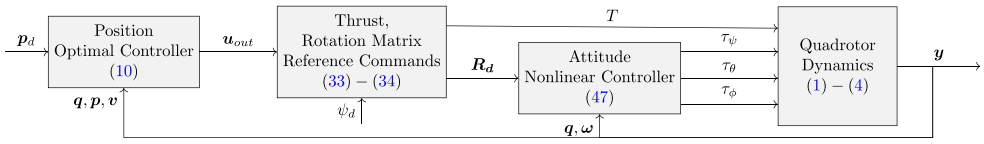

Fig. 2 Controller architecture

with $\dot{\boldsymbol{p}}_d = \boldsymbol{R}\boldsymbol{v}_d$, where $\boldsymbol{v}_d \in \mathbb{R}^3$ is the desired velocity in $\{B\}$. Define the body velocity error as

$$\boldsymbol{e}_{\boldsymbol{v}} = \boldsymbol{v} - \boldsymbol{v}_d. \tag{6}$$

In order to achieve zero steady-state error and to add robustness to model uncertainties, an integral feedback of the position error is taken into account

$$\dot{\boldsymbol{\eta}} = \boldsymbol{e}_{\boldsymbol{p}}. \tag{7}$$

Hence, by taking the derivative of Eqs. 5-6, considering the position system Eqs. 1-2 and the integral dynamic Eq. 7, the position tracking system is defined as

$$\begin{bmatrix} \dot{\boldsymbol{e}}_{\boldsymbol{p}} \\ \dot{\boldsymbol{e}}_{\boldsymbol{v}} \\ \dot{\boldsymbol{\eta}} \end{bmatrix} = \underbrace{\begin{bmatrix} \boldsymbol{0} & \boldsymbol{R} & \boldsymbol{0} \\ \boldsymbol{0} & -[\boldsymbol{\omega}\times] & \boldsymbol{0} \\ \boldsymbol{I} & \boldsymbol{0} & \boldsymbol{0} \end{bmatrix}}_{\boldsymbol{A}} \begin{bmatrix} \boldsymbol{e}_{\boldsymbol{p}} \\ \boldsymbol{e}_{\boldsymbol{v}} \\ \boldsymbol{\eta} \end{bmatrix} + \underbrace{\begin{bmatrix} \boldsymbol{0} \\ \boldsymbol{I} \\ \boldsymbol{0} \end{bmatrix}}_{\boldsymbol{B}} \boldsymbol{u}, \tag{8}$$

where

$$\boldsymbol{u} = -\frac{T}{m}\boldsymbol{e}_3 + \boldsymbol{R}^T\left(g\boldsymbol{e}_3 - \ddot{\boldsymbol{p}}_d\right) \tag{9}$$

and $\ddot{\boldsymbol{p}}_d \in \mathbb{R}^3$ is the desired inertial acceleration. The feedback control law proposed for the previous system is

$$\boldsymbol{u} = -\underbrace{\begin{bmatrix} \boldsymbol{R}^T\boldsymbol{K}_{\boldsymbol{p}} & \boldsymbol{R}^T\boldsymbol{K}_{\boldsymbol{v}}\boldsymbol{R} & \boldsymbol{R}^T\boldsymbol{K}_{\boldsymbol{\eta}} \end{bmatrix}}_{\boldsymbol{K}_{nl}} \begin{bmatrix} \boldsymbol{e}_{\boldsymbol{p}} \\ \boldsymbol{e}_{\boldsymbol{v}} \\ \boldsymbol{\eta} \end{bmatrix}, \tag{10}$$

where $\boldsymbol{K}_{\boldsymbol{p}}$, $\boldsymbol{K}_{\boldsymbol{v}}$, and $\boldsymbol{K}_{\boldsymbol{\eta}}$ are the steady-state LQR gain matrices $\in \mathbb{R}^{3\times3}$ corresponding to the LTI system

$$\begin{bmatrix} \dot{\boldsymbol{x}}_{\boldsymbol{p}} \\ \dot{\boldsymbol{x}}_{\boldsymbol{v}} \\ \dot{\boldsymbol{x}}_{\boldsymbol{\eta}} \end{bmatrix} = \underbrace{\begin{bmatrix} \boldsymbol{0} & \boldsymbol{I} & \boldsymbol{0} \\ \boldsymbol{0} & \boldsymbol{0} & \boldsymbol{0} \\ \boldsymbol{I} & \boldsymbol{0} & \boldsymbol{0} \end{bmatrix}}_{\boldsymbol{A}_l} \begin{bmatrix} \boldsymbol{x}_{\boldsymbol{p}} \\ \boldsymbol{x}_{\boldsymbol{v}} \\ \boldsymbol{x}_{\boldsymbol{\eta}} \end{bmatrix} + \underbrace{\begin{bmatrix} \boldsymbol{0} \\ \boldsymbol{I} \\ \boldsymbol{0} \end{bmatrix}}_{\boldsymbol{B}_l} \boldsymbol{u}. \tag{11}$$

In this section, it will be demonstrated that the feedback law Eq. 10 effectively stabilizes both the systems Eqs. 8 and 11. Additionally, it should be ensured that the control inputs provided by Eq. 10 closely match the desired inputs specified by Eq. 9 at all times. Since the only available input is the thrust T, the system is indeed underactuated. However, by assuming full control of $\boldsymbol{R}$, the trajectory tracking problem can simplified and transform it into the stabilization of a triple integrator [18]. This approach is adopted in this section to address the control challenges associated with underactuation.

Remark 1 The subsequent theorem follows from the existence of a Lyapunov transformation $\boldsymbol{T}(t)$, i.e. a bounded continuously differentiable matrix, for all t, with bounded derivative $\dot{\boldsymbol{T}}(t)$, and that admits inverse. Steady-state optimality for the proposed position controller is guaranteed in the sense that the solution for the problem at hand is found on the infinite time solution of the LTI Ricatti equation for the LTI system Eq. 11.

Theorem 1 Let the position error dynamics be described by Eq. 8. The closed-loop system that results from applying the feedback law Eq. 10 is globally exponential stable. Moreover, the feedback law is steady-state optimal in the sense that it minimizes the cost function

$$J = \int_0^\infty \frac{1}{2}\left(\boldsymbol{x}^T \underbrace{\begin{bmatrix} \boldsymbol{Q}_{\boldsymbol{p}} & \boldsymbol{0} & \boldsymbol{0} \\ \boldsymbol{0} & \boldsymbol{R}^T\boldsymbol{Q}_{\boldsymbol{v}}\boldsymbol{R} & \boldsymbol{0} \\ \boldsymbol{0} & \boldsymbol{0} & \boldsymbol{Q}_{\boldsymbol{\eta}} \end{bmatrix}}_{\boldsymbol{Q}} \boldsymbol{x} + \boldsymbol{u}^T \underbrace{\boldsymbol{R}^T\boldsymbol{R}_{\boldsymbol{p}}\boldsymbol{R}}_{\boldsymbol{R}_{\boldsymbol{u}}} \boldsymbol{u} \right) dt, \tag{12}$$

where $\boldsymbol{Q}_{\boldsymbol{p}}$, $\boldsymbol{Q}_{\boldsymbol{v}}$, and $\boldsymbol{Q}_{\boldsymbol{\eta}} \in \mathbb{R}^{3\times3}$ are symmetric positive semi-definite matrices, $\boldsymbol{R}_{\boldsymbol{p}} \in \mathbb{R}^{3\times3}$ is a symmetric, positive definite matrix, and $\boldsymbol{x} = \begin{bmatrix} \boldsymbol{e}_{\boldsymbol{p}}^T & \boldsymbol{e}_{\boldsymbol{v}}^T & \boldsymbol{\eta}^T \end{bmatrix}^T$.

Proof The proof follows the similar approach of the LQR. Applying the maximum principle theorem [19], to minimize the cost function Eq. 12 subject to the constraint Eq. 8, renders the optimal control law

$$\boldsymbol{u}^* = -\boldsymbol{R}_{\boldsymbol{u}}^{-1}\boldsymbol{B}^T\boldsymbol{\lambda}, \tag{13}$$

where $\boldsymbol{R}_{\boldsymbol{u}}$ is defined in Eq. 12, $\boldsymbol{\lambda} = \boldsymbol{P}\boldsymbol{x}$, and $\boldsymbol{P}$ is a square symmetric matrix governed by the matrix differential Ricatti equation

$$-\dot{\boldsymbol{P}} = \boldsymbol{P}\boldsymbol{A} + \boldsymbol{A}^T\boldsymbol{P} - \boldsymbol{P}\boldsymbol{B}\boldsymbol{R}_{\boldsymbol{u}}^{-1}\boldsymbol{B}^T\boldsymbol{P} + \boldsymbol{Q}. \tag{14}$$

Since the system Eq. 8 is time varying, $\boldsymbol{P}$ is also time varying. Nevertheless, consider the well-defined Lyapunov transfor-

mation $\boldsymbol{T}$ [20]

$$\boldsymbol{P} = \boldsymbol{T}\mathcal{P}\boldsymbol{T}^T,\ \boldsymbol{T} = \begin{bmatrix} \boldsymbol{I} & \boldsymbol{0} & \boldsymbol{0} \\ \boldsymbol{0} & \boldsymbol{R}^T & \boldsymbol{0} \\ \boldsymbol{0} & \boldsymbol{0} & \boldsymbol{I} \end{bmatrix},\ \dot{\boldsymbol{T}} = \begin{bmatrix} \boldsymbol{0} & \boldsymbol{0} & \boldsymbol{0} \\ \boldsymbol{0} & -[\boldsymbol{\omega}\times]\boldsymbol{R}^T & \boldsymbol{0} \\ \boldsymbol{0} & \boldsymbol{0} & \boldsymbol{0} \end{bmatrix}. \tag{15}$$

By application of Eq. 15 into Eq. 14, results the Ricatti equation for the LTI system Eq. 11

$$-\dot{\mathcal{P}} = \mathcal{P}\boldsymbol{A}_l + \boldsymbol{A}_l^T\mathcal{P} - \mathcal{P}\boldsymbol{B}_l\boldsymbol{R}_p^{-1}\boldsymbol{B}_l^T\mathcal{P} + \boldsymbol{Q}_l, \tag{16}$$

where $\boldsymbol{Q}_l = \boldsymbol{T}^T\boldsymbol{Q}\boldsymbol{T}$, $\boldsymbol{A}_l$ and $\boldsymbol{B}_l$ are defined in Eq. 11, and $\boldsymbol{R}_p$ is defined after Eq. 12. Consequently, at the infinity, $\dot{\mathcal{P}}_\infty = \boldsymbol{0}$ and the steady-state optimal control law $\boldsymbol{u}^*$ Eq. 13 can be rewritten as

$$\boldsymbol{u}^* = -\begin{bmatrix} \boldsymbol{R}^T\boldsymbol{K}_p & \boldsymbol{R}^T\boldsymbol{K}_v\boldsymbol{R} & \boldsymbol{R}^T\boldsymbol{K}_\eta \end{bmatrix}\begin{bmatrix} \boldsymbol{e}_p \\ \boldsymbol{e}_v \\ \boldsymbol{\eta} \end{bmatrix} \tag{17}$$

Thereby, $\boldsymbol{u}^*$ is the optimal control law that minimizes the cost function Eq. 12 for the position system Eq. 8. The globally exponential stability proof is now immediate. Consider the following well defined Lyapunov function

$$V_1(\boldsymbol{x}) = \boldsymbol{x}^T\boldsymbol{T}\mathcal{P}\boldsymbol{T}^T\boldsymbol{x}, \tag{18}$$

with time derivative given by

$$\begin{aligned} \dot{V}_1(\boldsymbol{x}) &= \frac{d}{dt}\left(\boldsymbol{x}^T\boldsymbol{T}\right)\mathcal{P}\boldsymbol{T}^T\boldsymbol{x} + \boldsymbol{x}^T\boldsymbol{T}\mathcal{P}\frac{d}{dt}\left(\boldsymbol{T}^T\boldsymbol{x}\right) \\ &= \boldsymbol{x}^T\left(\boldsymbol{A}_{cl}^T\boldsymbol{T} + \dot{\boldsymbol{T}}\right)\mathcal{P}\boldsymbol{T}^T\boldsymbol{x} \\ &\quad + \boldsymbol{x}^T\boldsymbol{T}\mathcal{P}\left(\boldsymbol{T}^T\boldsymbol{A}_{cl} + \dot{\boldsymbol{T}}^T\right)\boldsymbol{x} \\ &= \boldsymbol{x}^T\boldsymbol{T}\left(\boldsymbol{A}_l - \boldsymbol{B}\boldsymbol{K}_l\right)^T\mathcal{P}\boldsymbol{T}^T\boldsymbol{x} \\ &\quad + \boldsymbol{x}^T\boldsymbol{T}\mathcal{P}\left(\boldsymbol{A}_l - \boldsymbol{B}\boldsymbol{K}_l\right)\boldsymbol{T}^T\boldsymbol{x} \\ &= -\boldsymbol{x}^T\boldsymbol{T}\,\boldsymbol{Q}_l\boldsymbol{T}^T\boldsymbol{x}, \end{aligned} \tag{19}$$

with $\boldsymbol{A}_{cl} = \boldsymbol{A} - \boldsymbol{B}\boldsymbol{K}_{nl}$, $\boldsymbol{K}_{nl}$ defined in Eq. 10, and $\boldsymbol{K}_l = \begin{bmatrix} \boldsymbol{K}_p & \boldsymbol{0} & \boldsymbol{0} \\ \boldsymbol{0} & \boldsymbol{K}_v & \boldsymbol{0} \\ \boldsymbol{0} & \boldsymbol{0} & \boldsymbol{K}_\eta \end{bmatrix}$.

Thus, $V_1(\boldsymbol{x}) \geq 0$ and $\dot{V}_1(\boldsymbol{x}) \leq 0$, and, by the Theorem 4.9 in [21], the origin of the error system in closed-loop is globally asymptotically stable. Observe the following inequalities [21]

$$\begin{aligned} -\boldsymbol{x}^T\boldsymbol{T}\,\boldsymbol{Q}_l\boldsymbol{T}^T\boldsymbol{x} &\leq -\Lambda_{\min}(\boldsymbol{Q}_l)\boldsymbol{x}^T\boldsymbol{x}, \\ \boldsymbol{x}^T\boldsymbol{T}\mathcal{P}\boldsymbol{T}^T\boldsymbol{x} &\leq \Lambda_{\max}(\mathcal{P})\boldsymbol{x}^T\boldsymbol{x} \end{aligned}, \tag{20}$$

where $\Lambda_{\min}(\boldsymbol{Q}_l)$ and $\Lambda_{\max}(\mathcal{P})$ are both the minimum eigenvalue of $\boldsymbol{Q}_l$ and the maximum eigenvalue of $\mathcal{P}$, respectively, which are positive.

Define $\alpha = \frac{\Lambda_{\min}(\boldsymbol{Q}_l)}{\Lambda_{\max}(\mathcal{P})} > 0$ and apply Eqs. 20 to 19

$$\dot{V}_1(\boldsymbol{x}) \leq -\alpha V_1(\boldsymbol{x}), \tag{21}$$

Hence, the origin is globally exponentially stable. □

Bear in mind that, although the proposed controller guarantees steady-state optimality, by computing the solution for the Ricatti equation Eq. 16 and changing the controller gains accordingly during the transient period, optimality can be guaranteed for all t. For high bandwidth systems, such as a quadrotor UAV, the transient period is negligible. Additionally, the theorem shows that there is not required computing for all t the solution of the Ricatti equation for the linear time-variant system Eq. 8 to achieve steady-state optimality. The block diagram of the position controller is depicted in Fig. 3.

The position control is an underactuated problem with one control input and three output variables. The outer-loop is responsible to generate not only the desired thrust but also angular references. Noting that $\boldsymbol{u} = -\frac{T}{m}\boldsymbol{e}_3 + \boldsymbol{R}^T\left(g\boldsymbol{e}_3 - \ddot{\boldsymbol{p}}_d\right)$, and although T is a system input, the rotation matrix $\boldsymbol{R}^T$ is not and cannot be set arbitrarily. Nevertheless, the attitude variable $\boldsymbol{R}$ can be controlled by means of the attitude system Eqs. 3-4 and the input moments can be exploited to drive the thrust force to some intended direction. To deal with the coupling term, $\boldsymbol{u}$ can be divided, similarly as in [22], into

$$\boldsymbol{u} = \underbrace{-\frac{T}{m}\boldsymbol{e}_3 + \boldsymbol{R}_{\boldsymbol{d}}^T\left(g\boldsymbol{e}_3 - \ddot{\boldsymbol{p}}_d\right)}_{\boldsymbol{u}_d} - \underbrace{\left(\tilde{\boldsymbol{R}}^T - \boldsymbol{I}\right)\boldsymbol{R}^T\left(g\boldsymbol{e}_3 - \ddot{\boldsymbol{p}}_d\right)}_{\boldsymbol{\Delta}}, \tag{22}$$

where the term $\boldsymbol{\Delta} \in \mathbb{R}^3$ is a perturbation due to the attitude error control, $\boldsymbol{R}_{\boldsymbol{d}}$ is the desired rotation matrix, and $\tilde{\boldsymbol{R}} = \boldsymbol{R}^T\boldsymbol{R}_d$ describes the discrepancy between the vehicle attitude and the attitude command.

Remark 2 The stability proof present in this section does not hold for the coupling term $\boldsymbol{\Delta}$, which is a requisite for a hierarchical control scheme. Nevertheless, input-to-state stability (ISS) for the position closed-loop system, perturbed by $\boldsymbol{\Delta}$, is proved right after. Also, the integrator added to the plant attenuates the coupling term impact.

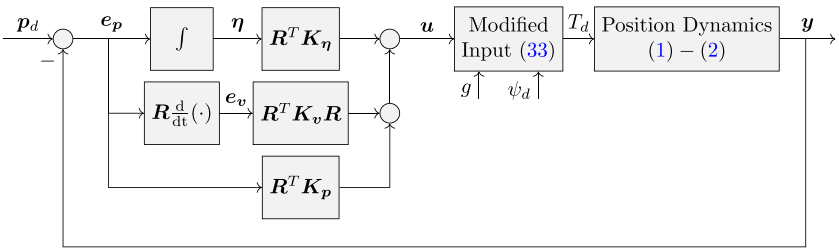

Fig. 3 Position controller block diagram

The position closed-loop system, perturbed by $\boldsymbol{\Delta}$, can be written as follows

$$\begin{bmatrix} \dot{\boldsymbol{e}}_p \\ \dot{\boldsymbol{e}}_v \\ \dot{\boldsymbol{\eta}} \end{bmatrix} = \underbrace{\begin{bmatrix} \boldsymbol{0} & \boldsymbol{R} & \boldsymbol{0} \\ -\boldsymbol{R}^T\boldsymbol{K}_p & -[\boldsymbol{\omega}\times] - \boldsymbol{R}^T\boldsymbol{K}_v\boldsymbol{R} & -\boldsymbol{R}^T\boldsymbol{K}_\eta \\ \boldsymbol{I} & \boldsymbol{0} & \boldsymbol{0} \end{bmatrix}}_{\boldsymbol{A}} \begin{bmatrix} \boldsymbol{e}_p \\ \boldsymbol{e}_v \\ \boldsymbol{\eta} \end{bmatrix} + \begin{bmatrix} \boldsymbol{0} \\ \boldsymbol{\Delta} \\ \boldsymbol{0} \end{bmatrix}, \quad (23)$$

Theorem 2 The position error dynamics Eq. 23 is ISS with input $\boldsymbol{\Delta}$, if $\exists\, k > 0 : \|\ddot{\boldsymbol{p}}_d\| \leq k,$ for all t.

Proof One can write the solution for the linear time varying system Eq. 23 in the form

$$\boldsymbol{x}(t) = \boldsymbol{\Phi}(t, t_0)\boldsymbol{x}_0 + \int_{t_0}^{t} \boldsymbol{\Phi}(t, \sigma)\boldsymbol{\Delta}(\sigma)d\sigma, \quad (24)$$

where $\boldsymbol{\Phi}$ is the state transition matrix, which is derived from the input free system, i.e., for $\boldsymbol{\Delta} = \boldsymbol{0}$. By Theorem 1, the input free system is uniformly asymptotically stable, which is equivalent to write

$$\exists\, \eta, \lambda > 0 : \|\Phi\,(t, t_0)\| \leq \eta e^{-\lambda[t-t_0]}, \text{ for all } t \geq t_0 \quad (25)$$

Apply the modulus to Eq. 24

$$\begin{aligned} \|\boldsymbol{x}(t)\| &\leq \eta e^{-\lambda[t-t_0]}\|\boldsymbol{x}_0\| + \int_{t_0}^{t} \eta e^{-\lambda[t-t_0]}\|\boldsymbol{\Delta}\|d\sigma \\ &\leq \underbrace{\eta e^{-\lambda[t-t_0]}\,\|\boldsymbol{x}_0\|}_{\beta(\|\boldsymbol{x}_0\|,t)} \\ &\quad + \underbrace{\frac{\eta\|\left(\tilde{\boldsymbol{R}}^T - \boldsymbol{I}\right)\|\|g\boldsymbol{e}_3 - \ddot{\boldsymbol{p}}_d\|_{t_0,\infty}}{\lambda}}_{\leq\gamma\left(\|\boldsymbol{\Delta}\|_{t_0,\infty}\right)}. \end{aligned} \quad (26)$$

According to Definition 4.7 in [21], and assuming that $\ddot{\boldsymbol{p}}_d$ is bounded, $\beta \in \mathcal{KL}$ and $\gamma \in \mathcal{K}$. Consequently, the closed-loop system Eq. 23 is ISS. □

Remark 3 The previous proof could also be accomplished by applying the Lyapunov transformation $\boldsymbol{T}$ to the closed-loop system Eq. 23, which would render an LTI system perturbed by a bounded perturbation $\boldsymbol{\Delta}$ that does not depend on the system states. Therefore, the LTI system is ISS. The transformation $\boldsymbol{T}$ is bounded and does not depend on the state variables, consequently the original system Eq. 23 has the ISS property.

One thing to bear in mind is that if $\boldsymbol{\Delta}$ converges to zero as $t \to \infty$, so does $\boldsymbol{x}(t)$, which would be the case if $\tilde{\boldsymbol{R}}^T(t) \to \boldsymbol{I}$ with time. This would imply GAS for the position closed-loop system Eq. 23.

Moreover, the desired rotation matrix $\boldsymbol{R_d}$ is obtained by equating $\boldsymbol{u}^*$ in Eq. 22 and the output of the feedback law $\boldsymbol{u}^*$ Eq. 17, which gives

$$\begin{aligned} \boldsymbol{u}^* &= -\frac{T}{m}\boldsymbol{e}_3 + \boldsymbol{R}_{\boldsymbol{d}}^T\,(g\boldsymbol{e}_3 - \ddot{\boldsymbol{p}}_d) \equiv \\ \underbrace{\boldsymbol{u}^* + \frac{T}{m}\boldsymbol{e}_3}_{\boldsymbol{u}_t} &= \underbrace{\boldsymbol{R_1}\boldsymbol{R_2}^T}_{\boldsymbol{R}_{\boldsymbol{d}}^T}\underbrace{(g\boldsymbol{e}_3 - \ddot{\boldsymbol{p}}_d)}_{\boldsymbol{\vartheta}} \equiv \boldsymbol{R_1}^T\boldsymbol{u}_t = \boldsymbol{R_2}^T\boldsymbol{\vartheta}, \end{aligned} \quad (27)$$

The idea is to find first $\boldsymbol{R_1}$ by imposing the following

$$\boldsymbol{R_1}^T\boldsymbol{u}_t = \|\boldsymbol{u}_t\|\,\boldsymbol{e_3} \equiv \qquad \boldsymbol{R_1}\boldsymbol{e_3} = \frac{\boldsymbol{u}_t}{\|\boldsymbol{u}_t\|}, \quad (28)$$

which is a similar problem as when the control is designed in the inertial frame. The rotation matrix can then be computed as

$$\boldsymbol{R_1} = \begin{bmatrix} \boldsymbol{b_1} & \boldsymbol{b_2} & \boldsymbol{b_3} \end{bmatrix}, \quad (29)$$

where $\boldsymbol{b_3} = \frac{\boldsymbol{u}_t}{\|\boldsymbol{u}_t\|}$, $\boldsymbol{b_2} = \frac{\boldsymbol{b_3}\times\boldsymbol{b_d}}{\|\boldsymbol{b_3}\times\boldsymbol{b_d}\|}$, $\boldsymbol{b_1} = \frac{\boldsymbol{b_2}\times\boldsymbol{b_3}}{\|\boldsymbol{b_2}\times\boldsymbol{b_3}\|}$, and $\boldsymbol{b_d} = \begin{bmatrix} 1 & 0 & 0 \end{bmatrix}^T$.

By computing $\boldsymbol{R_1}$ as in Eq. 29, the rotation matrix $\boldsymbol{R_2}$ can now be computed in a similar fashion since one can write $\boldsymbol{R_2}^T\boldsymbol{\vartheta}$ as follows

$$\boldsymbol{R_2}^T\boldsymbol{\vartheta} = \|\boldsymbol{u}_t\|\,\boldsymbol{e_3} \equiv \boldsymbol{R_2}\boldsymbol{e_3} = \frac{\boldsymbol{\vartheta}}{\|\boldsymbol{\vartheta}\|} \quad (30)$$

which can be solved in order to $\boldsymbol{R_2}$ as in Eq. 29, i.e.,

$$\boldsymbol{R_2} = \begin{bmatrix} \boldsymbol{d_1} & \boldsymbol{d_2} & \boldsymbol{d_3} \end{bmatrix}, \quad (31)$$

where $\boldsymbol{d_3} = \frac{\boldsymbol{\vartheta}}{\|\boldsymbol{\vartheta}\|}$, $\boldsymbol{d_2} = \frac{\boldsymbol{d_3}\times\boldsymbol{d_\psi}}{\|\boldsymbol{d_3}\times\boldsymbol{d_\psi}\|}$, $\boldsymbol{d_1} = \frac{\boldsymbol{d_2}\times\boldsymbol{d_3}}{\|\boldsymbol{d_2}\times\boldsymbol{d_3}\|}$, and $\boldsymbol{d_\psi} = \begin{bmatrix} cos(\psi_d) & \sin(\psi_d) & 0 \end{bmatrix}^T$, where ψ_d represents the desired yaw angle.

The relation given in Eqs. 28 and 30 fixes only two of the three degree of freedom of $\boldsymbol{R_1}$ and $\boldsymbol{R_2}$, respectively. The third degree of freedom, which is the rotation around the vectors $\boldsymbol{u}_t$ and $\boldsymbol{\vartheta}$, can be arbitrarily assigned according to attitude tracking objectives. For this particular case, the two third degree of freedom are defined by the assigned vectors $\boldsymbol{b_d}$ and $\boldsymbol{d_\psi}$.

The rotation matrix $\boldsymbol{R_2}$ represents the ideal desired rotation matrix according to the given trajectory. The rotation matrix $\boldsymbol{R_1}$, on the other hand, acts as a correction matrix that is dependent on the errors of the position system. The influence of $\boldsymbol{R_1}$ on $\boldsymbol{R_d}$ tends to diminish during the steady-state and increase during the transition states.

Lemma 1 Consider Eq. 27. If the following conditions are satisfied

$$\left\|\boldsymbol{u}^*\right\| < \|g\boldsymbol{e}_3 - \ddot{\boldsymbol{p}}_d\| > 0, \tag{32}$$

then it is always possible to extract the thrust magnitude from Eq. 27 as

$$T = m\left\|\sqrt{\|\boldsymbol{\vartheta}\|^2 - u_1^{*2} - u_2^{*2}} - u_3^*\right\|, \tag{33}$$

with $0 < T < 2m\|g\boldsymbol{e}_3 - \ddot{\boldsymbol{p}}_d\|$, and the desired rotation matrix $\boldsymbol{R_d}$ can be computed as

$$\boldsymbol{R_d} = \boldsymbol{R_2}\boldsymbol{R_1}^T. \tag{34}$$

Proof See Appendix A. □

Typically, the thrust is upper bounded, i.e. $T < T_{\max} \in \mathbb{R}_{>0}$, so being able to impose an upper constraint on it is advantageous. The following inequality can be found by imposing upper bounds on the thrust,

$$u_1^{*2} + u_2^{*2} + \left(u_3^{*2} + \frac{T_{\max}}{m}\right)^2 \geq \|g\boldsymbol{e}_3 - \ddot{\boldsymbol{p}}_d\|.$$

Remark 4 The use of saturation functions in the outer loop plays a critical role in avoiding singularities. Saturation functions are not considered throughout the paper. Nonetheless, any saturation function with guaranteed ISS for the position closed-loop system, such as several nested function found in the literature [23, 24], would serve this purpose.

The reference angular velocity $\boldsymbol{\omega}$ and its time derivative along the body x and y axis can be easily derived as functions of $\boldsymbol{u}_t$ and $\boldsymbol{\vartheta}$, and its time derivatives. As a matter of fact, it follows from $\boldsymbol{R_1}^T\dot{\boldsymbol{R}}_1\boldsymbol{e_3} = [\boldsymbol{\omega_1}\times]\boldsymbol{e_3}$ and $\boldsymbol{R_2}^T\dot{\boldsymbol{R}}_2\boldsymbol{e_3} = [\boldsymbol{\omega_2}\times]\boldsymbol{e_3}$ that

$$\begin{aligned}
\boldsymbol{\omega_1} &= \begin{bmatrix} -\boldsymbol{W}\boldsymbol{R_1}^T\frac{d}{dt}\left(\frac{\boldsymbol{u}_t}{\|\boldsymbol{u}_t\|}\right) \\ \omega_{13} \end{bmatrix}, \\
\boldsymbol{\omega_2} &= \begin{bmatrix} -\boldsymbol{W}\boldsymbol{R_2}^T\frac{d}{dt}\left(\frac{\boldsymbol{\vartheta}}{\|\boldsymbol{\vartheta}\|}\right) \\ \omega_{23} \end{bmatrix}, \\
\dot{\boldsymbol{\omega}}_1 &= \begin{bmatrix} -\boldsymbol{W}\left(-[\boldsymbol{\omega_1}\times]\boldsymbol{R_1}^T\frac{d}{dt}\left(\frac{\boldsymbol{u}_t}{\|\boldsymbol{u}_t\|}\right) + \boldsymbol{R_1}^T\frac{d^2}{dt^2}\left(\frac{\boldsymbol{u}_t}{\|\boldsymbol{u}_t\|}\right)\right) \\ \dot{\omega}_{13} \end{bmatrix}, \\
\dot{\boldsymbol{\omega}}_2 &= \begin{bmatrix} -\boldsymbol{W}\left(-[\boldsymbol{\omega_2}\times]\boldsymbol{R_2}^T\frac{d}{dt}\left(\frac{\boldsymbol{\vartheta}}{\|\boldsymbol{\vartheta}\|}\right) + \boldsymbol{R_2}^T\frac{d^2}{dt^2}\left(\frac{\boldsymbol{\vartheta}}{\|\boldsymbol{\vartheta}\|}\right)\right) \\ \dot{\omega}_{23} \end{bmatrix},
\end{aligned} \tag{35}$$

where $\boldsymbol{W} = \begin{bmatrix} 0 & 1 & 0 \\ -1 & 0 & 0 \end{bmatrix}$, and ω_{13}, ω_{23} and its derivatives are not subjected to constraints deriving from the position tracking objective. Finally, the desired angular velocity $\boldsymbol{\omega_d}$ and its derivative is defined in the lemma that follows

Lemma 2 The angular velocity $\boldsymbol{\omega}_d$ can be expressed as

$$\boldsymbol{\omega_d} = \boldsymbol{R_1}(\boldsymbol{\omega_2} - \boldsymbol{\omega_1}) \tag{36}$$

and

$$\|\boldsymbol{\omega}_d\| \leq \Omega_1 \; \forall \, t \geq 0, \;\; \Omega_1 \in \mathbb{R}_{\geq 0},$$

where $\boldsymbol{\omega_1}$ and $\boldsymbol{\omega_2}$ are defined in Eq. 35. Additionally, the angular acceleration $\dot{\boldsymbol{\omega}}_d$ can be expressed as

$$\dot{\boldsymbol{\omega}}_{\boldsymbol{d}} = \boldsymbol{R_1}(\dot{\boldsymbol{\omega}}_2 - \dot{\boldsymbol{\omega}}_1) + \boldsymbol{R_1}[\boldsymbol{\omega_1}\times](\boldsymbol{\omega_2} - \boldsymbol{\omega_1})$$

and

$$\|\dot{\boldsymbol{\omega}}_d\| \leq \Omega_2 \; \forall \, t \geq 0, \;\; \Omega_2 \in \mathbb{R}_{\geq 0},$$

where $\dot{\boldsymbol{\omega}}_1$ and $\dot{\boldsymbol{\omega}}_2$ are defined in Eq. 35.

Proof See Appendix B. □

From Lemmas 1-2, it is clear that the extracted attitude is time-varying, and that $\boldsymbol{\omega}_d$ and $\dot{\boldsymbol{\omega}}_d$ can be derived using the expressions of $\dot{\boldsymbol{u}}_t$ and $\ddot{\boldsymbol{u}}_t$, which are functions of available signals. The next section presents the attitude stabilization based on the quaternion parametrization. The quaternion space is topologically simpler than SO(3), which causes discontinuities when a memoryless maping to $\mathbb{S}^3$ is used. To prevent those undesirable effects, the path lifting mechanism presented in [25] is employed.

3.2 Quaternion Tracking Control

The attitude controller is designed via a similar procedure as in the position controller.

Suppose the desired orientation of the quadrotor is $\boldsymbol{q}_d = \begin{bmatrix}\boldsymbol{q}_{vd}^T & q_{4d}\end{bmatrix}^T = \begin{bmatrix}q_{1d} & q_{2d} & q_{3d} & q_{4d}\end{bmatrix}^T$. Define the quaternion error as follows

$$\boldsymbol{e}_q = \boldsymbol{\Xi}(\boldsymbol{q}_d)^T \boldsymbol{q}, \tag{37}$$

where $\boldsymbol{\Xi}(\boldsymbol{q}) = \begin{bmatrix} q_4 I_{3\times 3} + [\boldsymbol{q}_v\times] \\ -\boldsymbol{q}_v^{\mathrm{T}} \end{bmatrix}$.

Define the angular velocity error vector in the body frame, i.e.,

$$\boldsymbol{e}_\omega = \boldsymbol{\omega} - \boldsymbol{\Sigma}(\boldsymbol{e}_q)^{-1}\boldsymbol{\Sigma}(\boldsymbol{e}_q)^T\boldsymbol{\omega}_d \tag{38}$$

where $\boldsymbol{\Sigma}(\boldsymbol{e}_q) = \begin{bmatrix} \boldsymbol{q}_d^T\boldsymbol{q} & -e_{q3} & e_{q2} \\ e_{q3} & \boldsymbol{q}_d^T\boldsymbol{q} & -e_{q1} \\ -e_{q2} & e_{q1} & \boldsymbol{q}_d^T\boldsymbol{q} \end{bmatrix}$.

Take the derivative of Eqs. 37 and 38, and define the attitude tracking system by the kinematic differential equation

$$\dot{\boldsymbol{e}}_q = \frac{1}{2}\boldsymbol{\Sigma}(\boldsymbol{e}_q)\boldsymbol{e}_\omega \tag{39}$$

and by the dynamic equation

$$\dot{\boldsymbol{e}}_\omega = -\boldsymbol{J}^{-1}[\boldsymbol{\omega}\times]\boldsymbol{J}\boldsymbol{\omega} + \boldsymbol{J}^{-1}\boldsymbol{\tau} - \tfrac{\mathrm{d}}{\mathrm{dt}}\left(\boldsymbol{\Sigma}(\boldsymbol{e}_q)^{-1}\boldsymbol{\Sigma}(\boldsymbol{e}_q)^T\boldsymbol{\omega}_d\right). \tag{40}$$

Apply the following input transformation

$$\boldsymbol{\tau} = \boldsymbol{J}\left(\boldsymbol{J}^{-1}[\boldsymbol{\omega}\times]\boldsymbol{J}\boldsymbol{\omega} + \boldsymbol{\tau}_n + \tfrac{\mathrm{d}}{\mathrm{dt}}\left(\boldsymbol{\Sigma}(\boldsymbol{e}_q)^{-1}\boldsymbol{\Sigma}(\boldsymbol{e}_q)^T\boldsymbol{\omega}_d\right)\right) \tag{41}$$

and rewrite Eqs. 39-40 in state-space form as follows

$$\begin{bmatrix}\dot{\boldsymbol{e}}_q \\ \dot{\boldsymbol{e}}_\omega\end{bmatrix} = \begin{bmatrix}\boldsymbol{0} & \frac{1}{2}\boldsymbol{\Sigma}(\boldsymbol{e}_q) \\ \boldsymbol{0} & \boldsymbol{0}\end{bmatrix}\begin{bmatrix}\boldsymbol{e}_q \\ \boldsymbol{e}_\omega\end{bmatrix} + \begin{bmatrix}\boldsymbol{0} \\ \boldsymbol{\tau}_n\end{bmatrix}. \tag{42}$$

Consider the following nonlinear transformation of coordinates

$$\begin{bmatrix}\boldsymbol{e}_q \\ \boldsymbol{e}_\omega\end{bmatrix} = \boldsymbol{T}_q\begin{bmatrix}\boldsymbol{x}_q \\ \boldsymbol{x}_\omega\end{bmatrix}, \text{ with } \boldsymbol{T}_q = \begin{bmatrix}\boldsymbol{I} & \boldsymbol{0} \\ \boldsymbol{0} & \boldsymbol{\Sigma}(\boldsymbol{e}_q)^{-1}\end{bmatrix}, \tag{43}$$

with $|\boldsymbol{T}_q| = \boldsymbol{q}_d^T\boldsymbol{q}$. The determinant of $\boldsymbol{T}_q$ consists of the rotation cosine between the reference $\boldsymbol{q}_d$ and the nominal $\boldsymbol{q}$ quaternions. Consequently, the transformation matrix $\boldsymbol{T}_q$ is singular if and only if $\boldsymbol{q}_d$ and $\boldsymbol{q}$ are orthogonal.

Applying Eqs. 43 to 42 yields

$$\begin{bmatrix}\dot{\boldsymbol{x}}_q \\ \dot{\boldsymbol{x}}_\omega\end{bmatrix} = \begin{bmatrix}\boldsymbol{0} & \frac{1}{2}\boldsymbol{I} \\ \boldsymbol{0} & \boldsymbol{\Xi}(\boldsymbol{q}_d)^T\boldsymbol{\Xi}(\dot{\boldsymbol{q}})\boldsymbol{\Sigma}(\boldsymbol{e}_q)^{-1}\end{bmatrix}\begin{bmatrix}\boldsymbol{x}_q \\ \boldsymbol{x}_\omega\end{bmatrix} + \begin{bmatrix}\boldsymbol{0} \\ \boldsymbol{\Sigma}(\boldsymbol{e}_q)\end{bmatrix}\boldsymbol{\tau}_n. \tag{44}$$

Define the following input transformation law

$$\boldsymbol{\tau}_n = \boldsymbol{\Sigma}(\boldsymbol{e}_q)^{-1}\left(\boldsymbol{\tau}_l - \boldsymbol{\Xi}(\boldsymbol{q}_d)^T\boldsymbol{\Xi}(\dot{\boldsymbol{q}})\boldsymbol{\Sigma}(\boldsymbol{e}_q)^{-1}\boldsymbol{x}_\omega\right), \tag{45}$$

which transforms the system Eq. 44 into

$$\begin{bmatrix}\dot{\boldsymbol{x}}_q \\ \dot{\boldsymbol{x}}_\omega\end{bmatrix} = \begin{bmatrix}\boldsymbol{0} & \frac{1}{2}\boldsymbol{I} \\ \boldsymbol{0} & \boldsymbol{0}\end{bmatrix}\begin{bmatrix}\boldsymbol{x}_q \\ \boldsymbol{x}_\omega\end{bmatrix} + \begin{bmatrix}\boldsymbol{0} \\ \boldsymbol{I}\end{bmatrix}\boldsymbol{\tau}_l, \tag{46}$$

By inspection, the system is LTI and also controllable, which means that $\boldsymbol{\tau}_l$ can be given by an LQR feedback control law. Then, the control law for the nonlinear attitude tracking system Eqs. 39-40 is given by

$$\begin{aligned}\boldsymbol{\tau}(\boldsymbol{q}, \boldsymbol{q}_d, \boldsymbol{\omega}, \boldsymbol{\omega}_d) = \\ \boldsymbol{J}\boldsymbol{\Sigma}(\boldsymbol{e}_q)^{-1}\Big(\underbrace{\begin{bmatrix}-\boldsymbol{K}_{x_q} & -\boldsymbol{K}_{x_\omega}\boldsymbol{\Sigma}(\boldsymbol{e}_q)\end{bmatrix}\begin{bmatrix}\boldsymbol{e}_q \\ \boldsymbol{e}_\omega\end{bmatrix}}_{\boldsymbol{\tau}_l} - \boldsymbol{\Xi}(\boldsymbol{q}_d)^T\boldsymbol{\Xi}(\dot{\boldsymbol{q}})\boldsymbol{e}_\omega\Big) \\ + [\boldsymbol{\omega}\times]\boldsymbol{J}\boldsymbol{\omega} + \boldsymbol{J}\frac{\mathrm{d}}{\mathrm{dt}}\left(\boldsymbol{\Sigma}(\boldsymbol{e}_q)^{-1}\boldsymbol{\Sigma}(\boldsymbol{e}_q)^T\boldsymbol{\omega}_d\right),\end{aligned} \tag{47}$$

where $\boldsymbol{K}_{x_q}$ and $\boldsymbol{K}_{x_\omega}$ are the steady-state LQR gain matrices $\in \mathbb{R}^{3\times 3}$ corresponding to the LTI system Eq. 46.

Theorem 3 Let the attitude dynamics be described by Eqs. 39-40. The closed-loop system that results from applying the feedback law Eq. 47, assuming a sufficiently smooth trajectory such that $|\boldsymbol{T}_q| = \boldsymbol{q}_d^T\boldsymbol{q} \neq 0$, is almost globally exponentially stable.

Proof Apply the control law Eq. 47 to the attitude tracking system Eqs. 39-40, which is equivalent to

$$\begin{bmatrix}\dot{\boldsymbol{e}}_q \\ \dot{\boldsymbol{e}}_\omega\end{bmatrix} = \underbrace{\begin{bmatrix}\boldsymbol{0} & \frac{1}{2}\boldsymbol{\Sigma}(\boldsymbol{e}_q) \\ -\boldsymbol{\Sigma}(\boldsymbol{e}_q)^{-1}\boldsymbol{K}_{x_q} & -\boldsymbol{\Sigma}(\boldsymbol{e}_q)^{-1}\boldsymbol{K}_{x_\omega}\boldsymbol{\Sigma}(\boldsymbol{e}_q) - \boldsymbol{\Sigma}(\boldsymbol{e}_q)^{-1}\boldsymbol{\Xi}(\boldsymbol{q}_d)^T\boldsymbol{\Xi}(\dot{\boldsymbol{q}})\end{bmatrix}}_{\boldsymbol{A}_{cl}}\begin{bmatrix}\boldsymbol{e}_q \\ \boldsymbol{e}_\omega\end{bmatrix}, \tag{48}$$

Define $\boldsymbol{x}_2 = \begin{bmatrix}\boldsymbol{e}_q^T & \boldsymbol{e}_\omega^T\end{bmatrix}^T$. Choose the candidate Lyapunov function

$$V_2(\boldsymbol{x}_2) = \boldsymbol{x}_2^T\boldsymbol{T}_a\boldsymbol{\mathcal{P}}_a\boldsymbol{T}_a^T\boldsymbol{x}_2, \tag{49}$$

where $\boldsymbol{\mathcal{P}}_a$ is the steady-state covariance matrix of the Riccati equation for the LTI system Eq. 46, and $\boldsymbol{T}_a = \begin{bmatrix}\boldsymbol{I} & \boldsymbol{0} \\ \boldsymbol{0} & \boldsymbol{\Sigma}(\boldsymbol{e}_q)^T\end{bmatrix}$.

In steady-state, the Riccati equation verifies

$$\mathbf{0} = \boldsymbol{\mathcal{P}}_a \boldsymbol{A}_l + \boldsymbol{A}_l^T \boldsymbol{\mathcal{P}}_a + \boldsymbol{Q}_a. \tag{50}$$

Take the time derivative of Eq. 49

$$\dot{V}_2(\boldsymbol{x}_2) = -\boldsymbol{x}_2^T \boldsymbol{T}_a \boldsymbol{Q}_a \boldsymbol{T}_a^T \boldsymbol{x}_2, \tag{51}$$

As in the stability proof for the position system 1, there is an α such that $\alpha = \frac{\Lambda_{\min}(\boldsymbol{Q}_a)\Lambda_{\min}(\boldsymbol{T}_a^T \boldsymbol{T}_a)}{\Lambda_{\max}(\boldsymbol{\mathcal{P}}_a)\Lambda_{\max}(\boldsymbol{T}_a^T \boldsymbol{T}_a)} > 0$, which guarantees that

$$\dot{V}_2(\boldsymbol{x}_2) \leq -\alpha V_2(\boldsymbol{x}_2), \tag{52}$$

Hence, the origin is almost globally exponentially stable, since for $\boldsymbol{q}_d^T \boldsymbol{q} \neq 0$ the controller presents a singularity. □

The attitude error exhibits critical points that are influenced by the topology of SO(3). These critical points correspond to when $|\boldsymbol{T}_{\boldsymbol{q}}| = \boldsymbol{q}_{\boldsymbol{d}}^T \boldsymbol{q} = 0$. Due to the presence of these isolated critical points, it is not possible to design a globally stable continuous feedback controller in SO(3). Instead, achieving almost global stability is the best that can be accomplished through continuous feedback for the closed-loop system, as demonstrated in [26].

The block diagram of the attitude controller is depicted in Fig. 4.

4 Stability Analysis of the Architecture

Assuming that the condition Eq. 32 is satisfied, hence is always possible to extract the thrust, desired rotation matrix, $\boldsymbol{\omega}_d$, and $\dot{\boldsymbol{\omega}}_d$, which are all bounded signals according to Lemma 1-2. Then, from Theorem 2, the position closed-loop system Eq. 23 is ISS, and from Theorem 3, the attitude closed-loop system Eq. 48 is uniformly asymptotically stable. Consequently, the desired tracking objective for the whole system can be accomplished [27, Corollary B.3.3], and the perturbation term $\boldsymbol{\Delta} \to 0$ asymptotically as $t \to \infty$, which implies that $\boldsymbol{x}_1$ converges to zero.

A stronger proof, which guarantees almost uniform exponential stability for the combined system, can be achieved by forcing bounds on $\boldsymbol{Q_l}$ and $\boldsymbol{Q_a}$.

Let the Lyapunov function for the combined system be given by

$$V = V_1 + V_2. \tag{53}$$

Take the derivative Eq. 53 and account for the interconnection term $\boldsymbol{\Delta}$, i.e.,

$$\dot{V} = -\boldsymbol{x}_1^T \boldsymbol{T}\, \boldsymbol{Q}_l \boldsymbol{T}^T \boldsymbol{x}_1 - \boldsymbol{x}_2^T \boldsymbol{T}_a \boldsymbol{Q}_a \boldsymbol{T}_a^T \boldsymbol{x}_2 - 2\boldsymbol{x}_1^T \boldsymbol{T} \boldsymbol{K}_{\boldsymbol{\Delta}} \boldsymbol{R} \boldsymbol{\Delta}, \tag{54}$$

where $\boldsymbol{K}_{\boldsymbol{\Delta}} = \begin{bmatrix} \boldsymbol{\mathcal{P}}_2 \\ \boldsymbol{\mathcal{P}}_4 \\ \boldsymbol{\mathcal{P}}_5^T \end{bmatrix} \in \mathbb{R}^{9\times 3}$, with $\boldsymbol{\mathcal{P}} = \begin{bmatrix} \boldsymbol{\mathcal{P}}_1 & \boldsymbol{\mathcal{P}}_2 & \boldsymbol{\mathcal{P}}_3 \\ \boldsymbol{\mathcal{P}}_2^T & \boldsymbol{\mathcal{P}}_4 & \boldsymbol{\mathcal{P}}_5 \\ \boldsymbol{\mathcal{P}}_3^T & \boldsymbol{\mathcal{P}}_5^T & \boldsymbol{\mathcal{P}}_6 \end{bmatrix}$.

The error Eq. 37 verifies [28]

$$\tilde{\boldsymbol{R}} = \left[\left(q_{4e}^2 - \boldsymbol{e}_{\boldsymbol{q}}^{\mathrm{T}} \boldsymbol{e}_{\boldsymbol{q}} \right) \boldsymbol{I} + 2\boldsymbol{e}_{\boldsymbol{q}} \boldsymbol{e}_{\boldsymbol{q}}^{\mathrm{T}} - 2q_{4e} \left[\boldsymbol{e}_{\boldsymbol{q}} \times \right] \right]. \tag{55}$$

One may rewrite $\boldsymbol{\Delta}$, using Eq. 55, as follows

$$\boldsymbol{\Delta} = -2 \left([\boldsymbol{e}_q \times] + q_{4e} \boldsymbol{I} \right) [\boldsymbol{\vartheta} \times] \boldsymbol{e}_q, \tag{56}$$

where $\boldsymbol{\vartheta}$ is defined in Eq. 27, such that $\dot{V}$ can be given by

$$\begin{aligned}
\dot{V} =& -\boldsymbol{x}_1^T \boldsymbol{T}\, \boldsymbol{Q}_l \boldsymbol{T}^T \boldsymbol{x}_1 - \boldsymbol{x}_2^T \boldsymbol{T}_a \boldsymbol{Q}_a \boldsymbol{T}_a^T \boldsymbol{x}_2 \\
&+ 4\boldsymbol{x}_1^T \boldsymbol{T} \boldsymbol{K}_{\boldsymbol{\Delta}} \boldsymbol{R} \left([\boldsymbol{e}_q \times] + q_{4e} \boldsymbol{I} \right) [\boldsymbol{\vartheta} \times] \boldsymbol{e}_q \\
\leq& -\Lambda_{\min}(\boldsymbol{Q}_l) \|\boldsymbol{x}_1\|^2 - \Lambda_{\min}(\boldsymbol{Q}_a) \|\boldsymbol{x}_2\|^2 \\
&+ \underbrace{4\sqrt{2}\sqrt{2 + q_{4e}^2} \Lambda_{\max}(\boldsymbol{\mathcal{P}}_2) \|\boldsymbol{\vartheta}\|}_{\boldsymbol{\Upsilon}_1} \|\boldsymbol{e}_p\| \|\boldsymbol{e}_q\| \\
&+ \underbrace{4\sqrt{2}\sqrt{2 + q_{4e}^2} \Lambda_{\max}(\boldsymbol{\mathcal{P}}_4) \|\boldsymbol{\vartheta}\|}_{\boldsymbol{\Upsilon}_2} \|\boldsymbol{e}_v\| \|\boldsymbol{e}_q\| \\
&+ \underbrace{4\sqrt{2}\sqrt{2 + q_{4e}^2} \Lambda_{\max}(\boldsymbol{\mathcal{P}}_5) \|\boldsymbol{\vartheta}\|}_{\boldsymbol{\Upsilon}_3} \|\boldsymbol{\eta}\| \|\boldsymbol{e}_q\| \\
\leq& -\begin{bmatrix} \|\boldsymbol{x}_1\| \\ \|\boldsymbol{x}_2\| \end{bmatrix}^T \begin{bmatrix} \Lambda_{\min}(\boldsymbol{Q}_l) & -\frac{1}{2}(\boldsymbol{\Upsilon}_1 + \boldsymbol{\Upsilon}_2 + \boldsymbol{\Upsilon}_3) \\ -\frac{1}{2}(\boldsymbol{\Upsilon}_1 + \boldsymbol{\Upsilon}_2 + \boldsymbol{\Upsilon}_3) & \Lambda_{\min}(\boldsymbol{Q}_a) \end{bmatrix} \begin{bmatrix} \|\boldsymbol{x}_1\| \\ \|\boldsymbol{x}_2\| \end{bmatrix}.
\end{aligned} \tag{57}$$

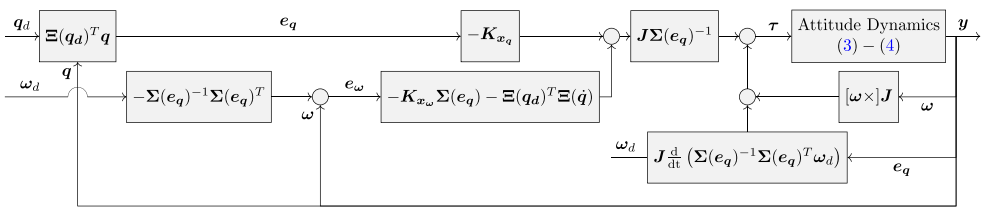

Fig. 4 Attitude controller block diagram

The previous Lyapunov function derivative is negative definite for

$$\begin{aligned} &\Lambda_{\min}(\boldsymbol{Q}_a) > 0 \text{ and} \\ &\Lambda_{\min}(\boldsymbol{Q}_l)\Lambda_{\min}(\boldsymbol{Q}_a) - \frac{1}{4}(\boldsymbol{\Upsilon}_1 + \boldsymbol{\Upsilon}_2 + \boldsymbol{\Upsilon}_3)^2 > 0, \end{aligned} \tag{58}$$

which, according to Theorem 4.10 in [21], guarantees exponential stability for the combined system. By tuning the LQR parameters $\boldsymbol{Q}$ and $\boldsymbol{R}$, the previous inequalities can be accomplished. Note that by fixing $\boldsymbol{Q}$, $\boldsymbol{\Upsilon}_i$ can be made sufficiently small by increasing the input action control $\boldsymbol{R}$.

Less restrictive inequalities can be found to guarantee exponential stability. One may write the following inequality

$$\dot{V} \leq -\begin{bmatrix} \|\boldsymbol{e_p}\| \\ \|\boldsymbol{e_v}\| \\ \|\boldsymbol{\eta}\| \\ \|\boldsymbol{e_q}\| \\ \|\boldsymbol{e_\omega}\| \end{bmatrix}^T \begin{bmatrix} \Lambda_{\min}(\boldsymbol{Q}_p) & \boldsymbol{0} & \boldsymbol{0} & -\frac{1}{2}\boldsymbol{\Upsilon}_1 & \boldsymbol{0} \\ \boldsymbol{0} & \Lambda_{\min}(\boldsymbol{Q}_v) & \boldsymbol{0} & -\frac{1}{2}\boldsymbol{\Upsilon}_2 & \boldsymbol{0} \\ \boldsymbol{0} & \boldsymbol{0} & \Lambda_{\min}(\boldsymbol{Q}_\eta) & -\frac{1}{2}\boldsymbol{\Upsilon}_3 & \boldsymbol{0} \\ -\frac{1}{2}\boldsymbol{\Upsilon}_1 & -\frac{1}{2}\boldsymbol{\Upsilon}_2 & -\frac{1}{2}\boldsymbol{\Upsilon}_3 & \Lambda_{\min}(\boldsymbol{Q}_q) & \boldsymbol{0} \\ \boldsymbol{0} & \boldsymbol{0} & \boldsymbol{0} & \boldsymbol{0} & \Lambda_{\min}(\boldsymbol{Q}_\omega) \end{bmatrix} \begin{bmatrix} \|\boldsymbol{e_p}\| \\ \|\boldsymbol{e_v}\| \\ \|\boldsymbol{\eta}\| \\ \|\boldsymbol{e_q}\| \\ \|\boldsymbol{e_\omega}\| \end{bmatrix}, \tag{59}$$

which is negative definite for

$$\begin{aligned} &\Lambda_{\min}(\boldsymbol{Q}_\omega) > 0, \ \Lambda_{\min}(\boldsymbol{Q}_q) > 0, \\ &J_1 = \Lambda_{\min}(\boldsymbol{Q}_\eta)\Lambda_{\min}(\boldsymbol{Q}_q) - \frac{1}{4}\boldsymbol{\Upsilon}_3^2 > 0, \\ &J_2 = \Lambda_{\min}(\boldsymbol{Q}_v)J_1 - \frac{1}{4}\Lambda_{\min}(\boldsymbol{Q}_\eta)\boldsymbol{\Upsilon}_2^2 > 0, \\ &J_3 = \Lambda_{\min}(\boldsymbol{Q}_p)J_2 - \frac{1}{4}\Lambda_{\min}(\boldsymbol{Q}_v)\Lambda_{\min}(\boldsymbol{Q}_\eta)\boldsymbol{\Upsilon}_1^2 > 0. \end{aligned} \tag{60}$$

A simple procedure can now be derived to render the combined system exponentially stable, i.e.,

1. Define $\boldsymbol{Q_\eta}$, $\boldsymbol{Q_q}$ and $\boldsymbol{R_p}$ such that $J_1 > 0$;
2. Define $\boldsymbol{Q_v}$ such that $J_2 > 0$;
3. Define $\boldsymbol{Q_p}$ such that $J_3 > 0$, and choose $\boldsymbol{R_q}$ to fulfil the input action.

Although the combined system has guaranteed uniform stability, as stated in the beginning of Section 4, the conditions present in Eq. 60 guarantees exponential convergence rate of $\boldsymbol{x}_1$ and $\boldsymbol{x}_2$ to zero.

Additionally, one can add the integral of the quaternion error, i.e.

$$\boldsymbol{e_{qi}} = \int \boldsymbol{e_q}\, dt, \tag{61}$$

as a state variable, to cope with unmodelled system behaviour and increase the system robustness. The incorporation of the state variable (61) enhances the performance of the control system by eliminating steady-state errors caused by constant disturbances or reference input commands.

Remark 5 The presence of plant integrators enables the control system to handle constant uncertainties in the dynamical model. As long as these uncertainties remain constant, exponential stability of the position and attitude error is maintained. However, when dealing with nonlinear uncertainties, such as a biased mass or moment of inertia, additional measures are required. The introduction of a nonlinear integrative or adaptive term in the control system can help restore exponential stability and address the effects of these nonlinear uncertainties [29].

The addition of this new variable does not alter the trajectory system properties, as it would just add the negative quadratic term $\Lambda_{\min}(\boldsymbol{Q}_{qi}) \left\|\boldsymbol{e_{qi}}\right\|^2$ to the derivative of the Lyapunov function $\dot{V}$ Eq. 59. Moreover, an augmented LTI system, similar to Eq. 46, is used to take into account the new variable, i.e.

$$\begin{bmatrix} \dot{\boldsymbol{x}}_{\boldsymbol{q}} \\ \dot{\boldsymbol{x}}_{\boldsymbol{\omega}} \\ \dot{\boldsymbol{e}}_{\boldsymbol{qi}} \end{bmatrix} = \begin{bmatrix} \boldsymbol{0} & \frac{1}{2}\boldsymbol{I} & \boldsymbol{0} \\ \boldsymbol{0} & \boldsymbol{0} & \boldsymbol{0} \\ \boldsymbol{I} & \boldsymbol{0} & \boldsymbol{0} \end{bmatrix} \begin{bmatrix} \boldsymbol{x}_{\boldsymbol{q}} \\ \boldsymbol{x}_{\boldsymbol{\omega}} \\ \boldsymbol{e}_{\boldsymbol{qi}} \end{bmatrix} + \begin{bmatrix} \boldsymbol{0} \\ \boldsymbol{I} \\ \boldsymbol{0} \end{bmatrix} \boldsymbol{\tau}_{\boldsymbol{l}} \tag{62}$$

which allows to substitute the feedback control law $\boldsymbol{\tau_l}$ present in Eq. 47 for

$$\boldsymbol{\tau_{li}} = \begin{bmatrix} -\boldsymbol{K}_{\boldsymbol{x_q}} & -\boldsymbol{K}_{\boldsymbol{x_\omega}}\boldsymbol{\Sigma}(\boldsymbol{e_q}) & -\boldsymbol{K}_{\boldsymbol{e_{qi}}} \end{bmatrix} \begin{bmatrix} \boldsymbol{e_q} \\ \boldsymbol{e_\omega} \\ \boldsymbol{e_{qi}} \end{bmatrix}, \tag{63}$$

where $\boldsymbol{K}_{\boldsymbol{e_{qi}}}$ is the steady-state LQR gain matrix $\in \mathbb{R}^{3\times 3}$ for the variable $\boldsymbol{e_{qi}}$ corresponding to the LTI system Eq. 62.

5 Results and Discussion

The quadrotor selected to assess the proposed controller performance was an AR. Drone 2.0, which offers the capability to deploy custom software that overrides the factory control through a Simulink package [30], granting access to the Pulse Width Modulation (PWM) of each motor. The vehicle is equipped with four propellers. The dynamics of the system can be described by Eqs. 1-4, where the resultant thrust T and torque $\boldsymbol{\tau}$ can be determined as a function of the four thrusts T_i, $i = 1, 2, 3, 4$, produced by four different propellers, for instance

$$\begin{bmatrix} T \\ \boldsymbol{\tau} \end{bmatrix} = \begin{bmatrix} 1 & 1 & 1 & 1 \\ l & -l & -l & l \\ -l & -l & l & l \\ c_d & -c_d & c_d & -c_d \end{bmatrix} \begin{bmatrix} T_1 \\ T_2 \\ T_3 \\ T_4 \end{bmatrix}, \tag{64}$$

where l represents the distance from the propeller axis to the center of gravity of the body, and $c_d = 0.0033m$ [31] is a parameter that linearly relates the thrust of each motor to the moment produced along the axis of the rotor. The relevant physical quantities are $m = 0.5Kg$, $\boldsymbol{J} = \text{diag}\,(0.0027, 0.0029, 0.0053)\ Kg.m^2$ [31], $l = 0.127m$. The simulation and the control onboard of the quadrotor is ran at a frequency of 100 Hz.

In the next two subsections, simulation and experimental results are shown to assess the feasibility of the control strategy proposed, Eqs. 33 and 47-63, designed in Section 3.

5.1 Simulation Results

The vehicle starts with the states at zero and takes off at $t = 2s$. At $t = 10s$, the following "8-shaped" curve trajectory is generated

$$\begin{aligned} \boldsymbol{p}_d(t) &= \begin{bmatrix} 2\cos\left(\frac{3\pi}{32}t\right) \\ \sin\left(\frac{3\pi}{16}t\right) \\ \frac{1}{3}\cos\left(\frac{3\pi}{32}t\right) \end{bmatrix} + \begin{bmatrix} -2 \\ 0 \\ -1.13 \end{bmatrix}, \text{ with} \\ \psi_d(t) &= 2\text{atan2}\left(\sqrt{\dot{p}_{d1}^2 + \dot{p}_{d2}^2} - \dot{p}_{d1}\ ,\ \dot{p}_{d2}\right). \end{aligned} \tag{65}$$

The controller parameters are presented in Table 1. The use of the LTI systems Eqs. 11 and 46 governed by the conditions in Eq. 60, enables a straightforward procedure for the tuning of the control gains. To test for robustness of the proposed tracking law, disturbances and parameter uncertainties have been taken into account. Specifically, the transformation Eq. 64 from $\boldsymbol{\tau}$ to T_i is assumed to be biased by some constant, white noise is added to every measurement to mimic sensor noise. Finally, it is considered a moment of inertia 10% higher than the nominal one.

The simulation results are displayed from Figs. 5 to 7. The actual 3D and 2D trajectory and the desired path are shown in Figs. 5 and 7, respectively, and exhibit the system converging to the reference path. As seen in Fig. 8, the tracking errors exponentially converge to zero. The transient convergence to the path occurs within 3s. The controller presents zero

Table 1 Controller parameters

Subsystem	Q_l	R_l
e_p	$\text{diag}\,(5, 5, 2.5) \times 10^3$	
e_v	$\text{diag}\,(3, 3, 3) \times 10^3$	110
e_η	$\text{diag}\,(8, 8, 8) \times 10$	
e_q	$\text{diag}\,(65, 65, 150) \times 10^4$	
e_ω	$\text{diag}\,(5, 5, 2) \times 10^4$	92
e_{qi}	$\text{diag}\,(30, 30, 30) \times 10^5$	

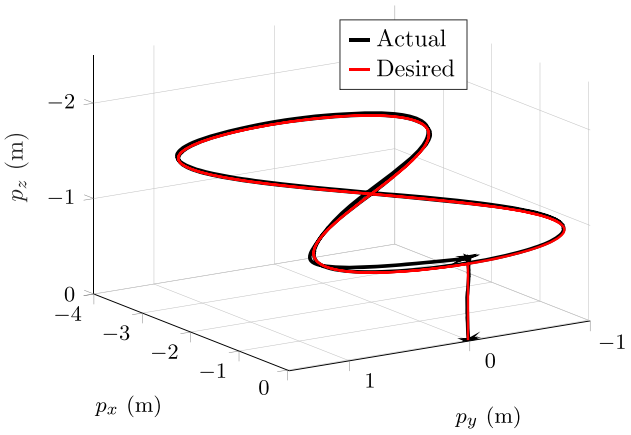

Fig. 5 Simulated spatial trajectory response with the proposed control approach

position and velocity errors in steady-state. The thrust and moments actuations are depicted in Fig. 6.

5.1.1 Performance test

In order to thoroughly assess the performance of the proposed controller, two distinct experiments were conducted in simulation.

The first experiment involved intentionally introducing variations of ±30% in the nominal moment of inertia $\boldsymbol{J}$. Figure 9 presents the results of the experiment, showing that there is minimal difference in both the position and attitude errors when varying the moment of inertia. Despite the controller's dependence on the accurate estimation of $\boldsymbol{J}$ to mitigate cross-term effects in the dynamics, the results

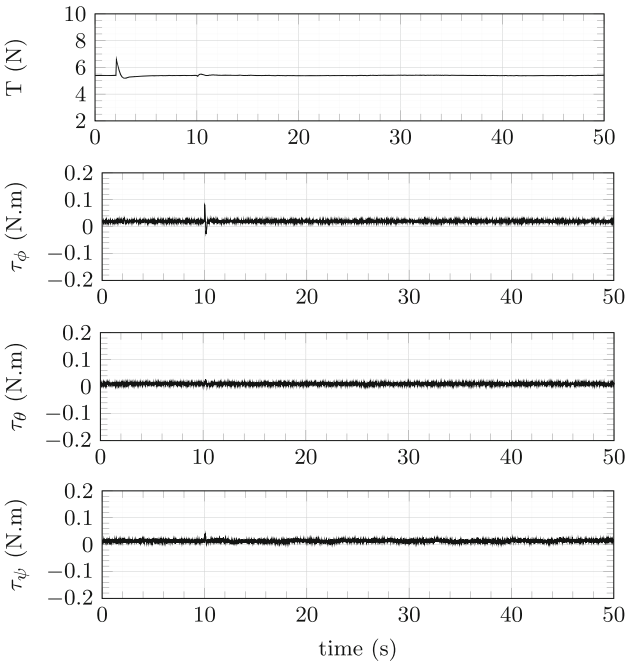

Fig. 6 Simulated actuations of the quadrotor

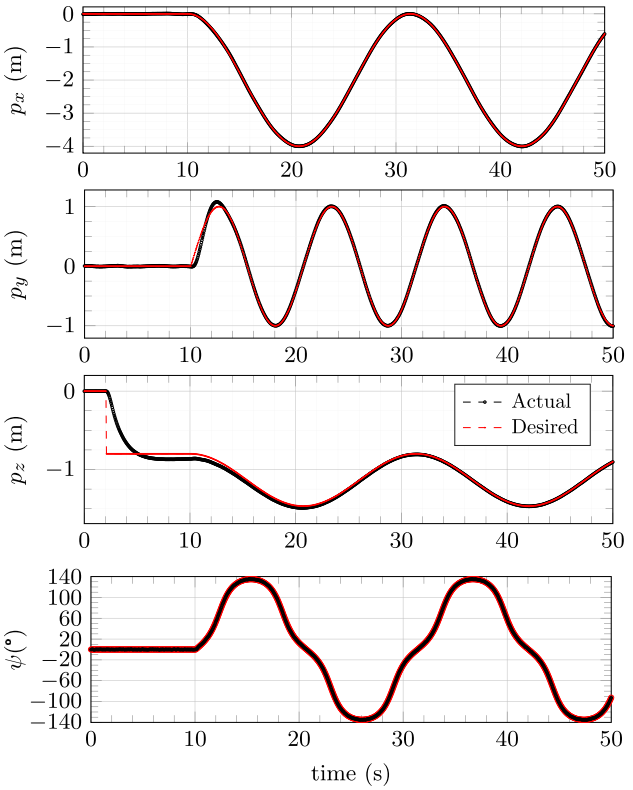

Fig. 7 Simulation responses obtained with the quadrotor during trajectory tracking with the proposed nonlinear control approach

demonstrate its ability to handle uncertainties in the inertia, primarily attributed to the integrator component. This finding underscores the robustness of the controller in compensating for variations in the moment of inertia and its effectiveness in achieving desirable control performance.

In the second experiment, a slung load mass m_p with length $l_p = 1m$ was attached to the center of mass of the vehicle, following the dynamics derived in [32]. This experiment aimed to examine the ability of the controller to stabilize the system with an additional dynamic coupling. The results of the experiment are shown in Fig. 10. One can notice that by considering a pendulum of mass up to $m_p = 50g$, i.e. 10% of the vehicle's mass, there is minimal difference in terms of position and attitude error. However, as the ratio between masses increases, the attitude angles, particularly the roll and pitch angles, exhibit more fluctuations during the simulation, as observed in Fig. 10. This indicates that the proposed controller is able to cope with dynamic uncertainties to maintain consistent performance and to asymptotically stabilize the system.

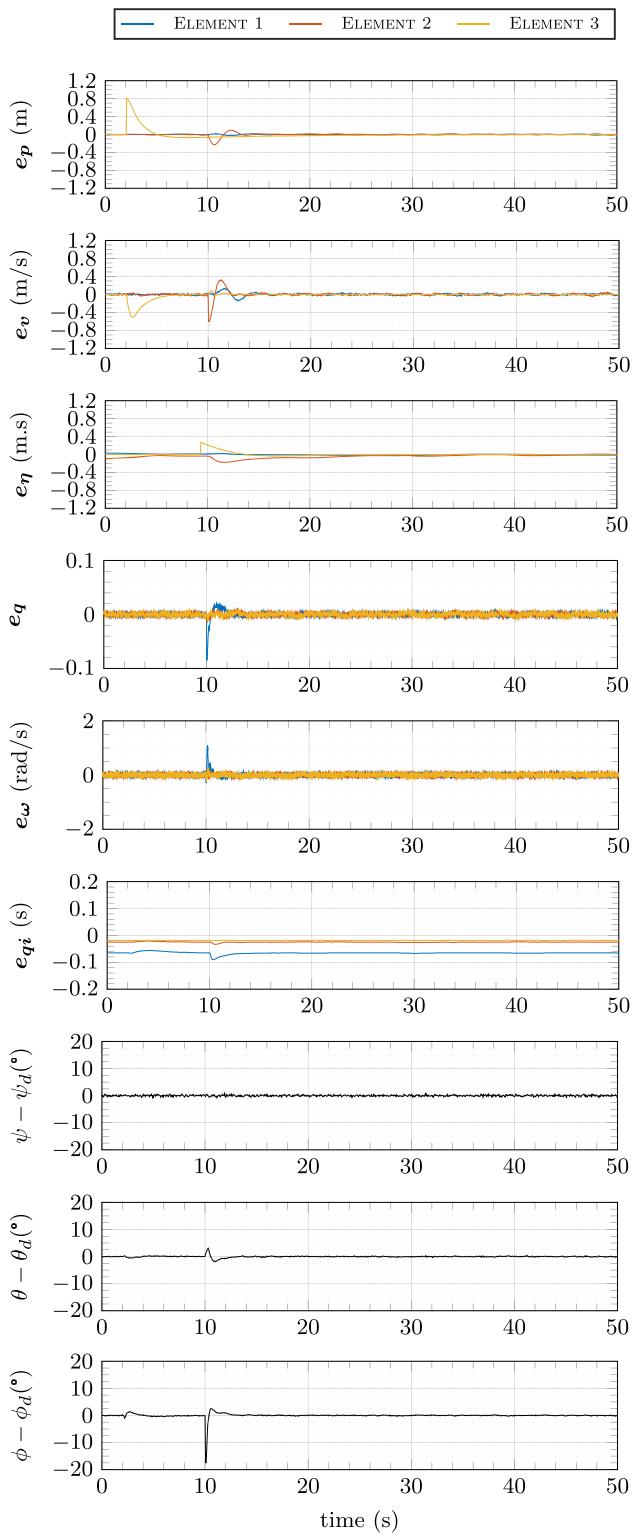

Fig. 8 Simulation errors

5.2 Experimental Results

The experimental results attained with the coupled position Eq. 33 and attitude controller Eqs. 47-63, onboard of an AR.Drone 2.0, are presented from Fig. 13-14. The controller is implemented on-board the vehicle using a Simulink package [30], which enables compilation and deployment of

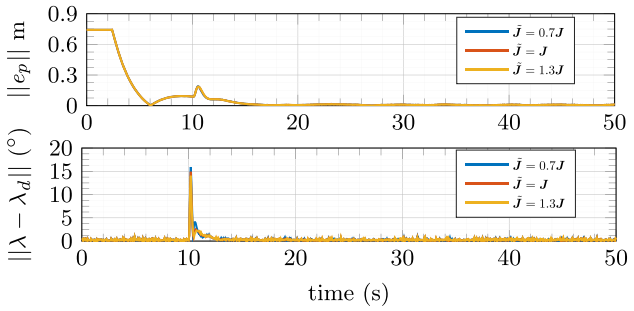

Fig. 9 Simulation error responses obtained in the moment of inertia variation test

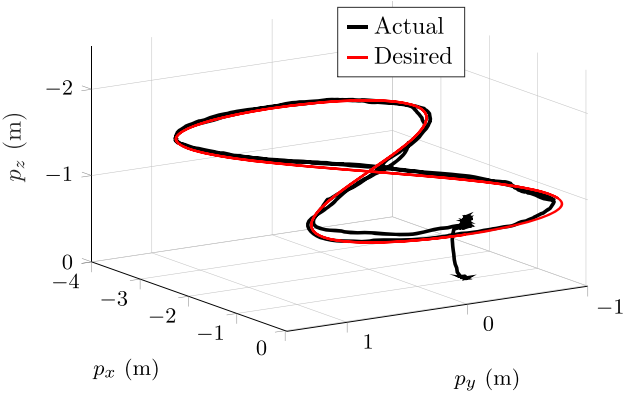

Fig. 11 Experimental spatial trajectory response with the proposed control approach

the controller. For the experiment, a position tracking system (Qualisys) alongside the onboard IMU and ultrasound of the vehicle has been employed to provide real-time accurate measurements of position, velocity, quaternion angles and angular velocity, at a rate of 100 Hz. To allow a fair comparison, the controller parameters and the path used in simulation is the same as for the real-time experiment.

The quadrotor lifts off at 2 s from the ground floor and aims to follow a desired path Eq. 65. The Figs. 11 and 13, show that the controller was successfully able to track the reference path displayed in red.

The actual trajectories are displayed in black. The transient convergence to the path occurs within 3 s and the steady-state is overall less than 10 cm. The system errors, depicted in Fig. 14, converge to zero and remain bounded. The actuations are plotted in Fig. 12. Despite the overlooked non-linearities in the dynamic model, the experimental results match properly with the simulation, see Figs. 7 and 13. The proposed control strategy demonstrates to be effective in practical applications. Furthermore, another similar experiment was recorded and the result can be seen in https://youtu.be/wcoelQo6Fjs.

5.2.1 Performance test - Slung load

To conduct a comprehensive assessment of the proposed controller's performance under laboratory conditions, two different slung load masses were affixed to the quadrotor setup to replicate the scenarios studied in simulations, see Fig. 15. The trajectory remained consistent with the one described in Eq. 65. However, a modification was made to the trajectory in the Z-axis by raising it by 30*cm* to prevent contact between the slung load and the ground, and only

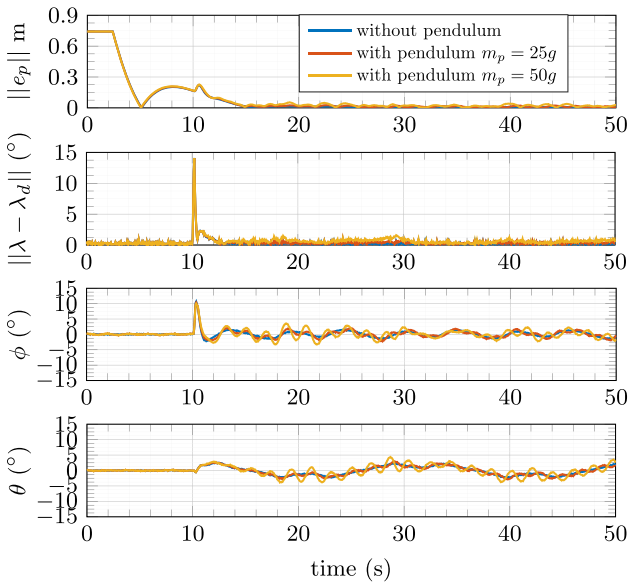

Fig. 10 Simulation responses obtained in the pendulum test with the control approach

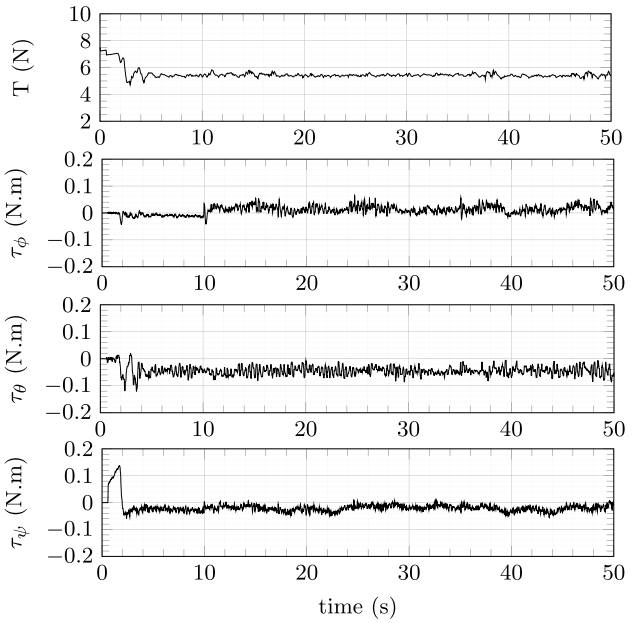

Fig. 12 Experimental actuations of the quadrotor

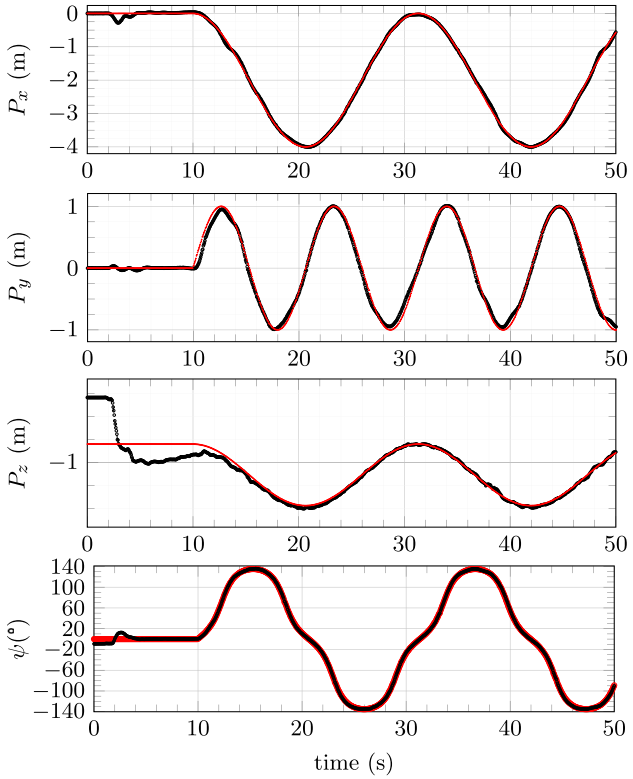

Fig. 13 Experimental responses obtained with the quadrotor during trajectory tracking

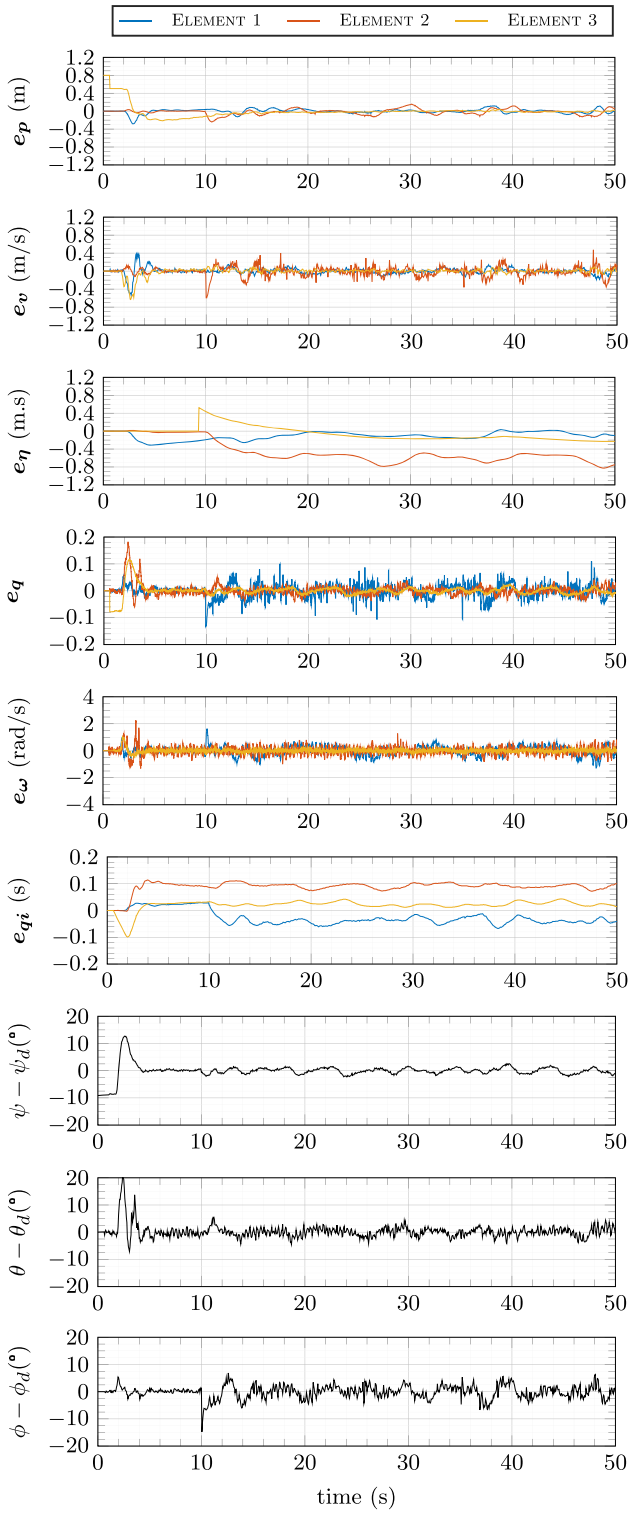

Fig. 14 Experimental errors

one lap was performed. The cable has the same length as in the simulation, $l_p = 1m$, while the slug load masses weight $m_{p1} = 21g$ and $m_{p2} = 49g$.

The experiment aimed to examine the ability of the controller to stabilize the system with an additional dynamic coupling in a laboratory environment. The results of the experiment are shown in Fig. 16. As observed in the results, the controller effectively handled the presence of the slung load, with only a marginal increase in position error noticed. Despite the simulations results of Fig. 10, the controller demonstrated its ability to handle both sets of pendulum masses, with minimal differences observed in the attitude angles compared to the experiment without the slung load, as depicted in Fig. 10. This underscores the capability of the proposed controller to manage the considered dynamic uncertainties, ensuring consistent performance, and asymptotically stabilizing the system. Furthermore, the experiments with the slung load were recorded and made available in https://youtu.be/NWmEOzTzzjc.

6 Conclusions

This paper presented a trajectory tracking controller for a quadrotor with steady-state optimal properties, developed on the sensor and quaternion spaces. The controller stabilizes the position and attitude of a rigid body robustly and almost globally asymptotically. The position dynamics are formulated in the body frame, which allows direct usage of

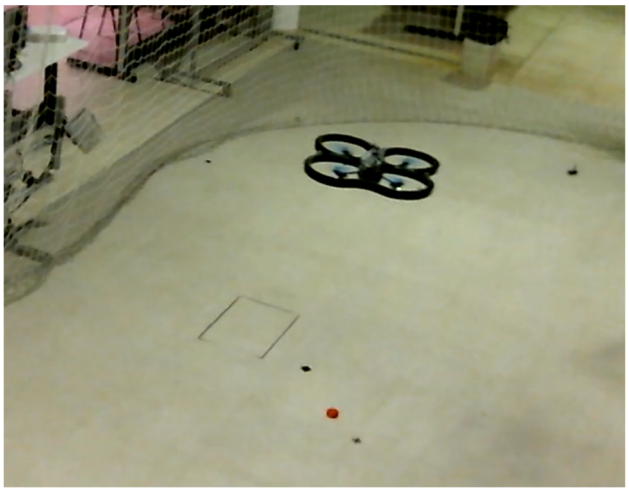

Fig. 15 Quadrotor carrying the pendulum in red with $m_p = 49g$ during the experiment

sensor measurements, such as the combination of IMU and optical flow. Through a specific set of transformation matrices, the position system is rendered LTI, allowing the exploit of linear control techniques that optimally stabilizes it. At first, position and attitude are addressed separately. The origin of the position controller exhibits exponential stability and ISS properties. The attitude controller, derived from a set of nonlinear transformations and input to state feedback, renders the attitude system almost globally stable. The technique enables the fine tuning of the attitude controller through

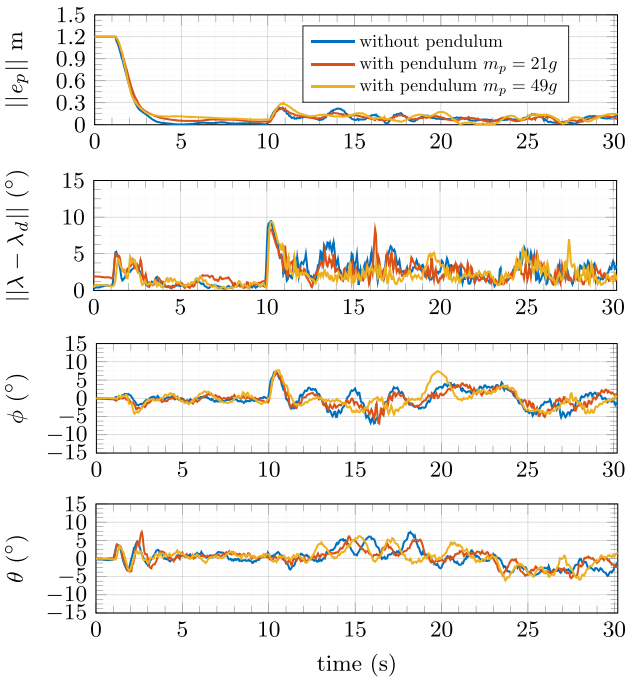

Fig. 16 Experimental responses obtained in the pendulum test with the proposed control approach

a LTI system, while maintaining its properties. Furthermore, by analysis of the Lyapunov function for the combined system, and accounting for the interconnection term, the overall closed-loop system exhibits exponential stability properties when certain conditions are satisfied. Experimental and simulation results were shown to assess the performance of the proposed controller.

Appendix A: Proof of Lemma 1

The thrust T is retrieved by setting

$$\|u_t\| = \|v\| \equiv$$
$$T = m\left|\sqrt{\|\boldsymbol{\vartheta}\|^2 - u_1^{*2} - u_2^{*2}} - u_3^*\right| > 0$$

Furthermore, and due to the vehicle capabilities, the thrust cannot be negative, which implies

$$T > 0 \implies \left\|\boldsymbol{u}^*\right\| < \|g\boldsymbol{e}_3 - \ddot{\boldsymbol{p}}_d\|.$$

Then, in order to compute $\boldsymbol{R}_1$ Eq. 28 and $\boldsymbol{R}_2$ Eq. 30 the norm of $\boldsymbol{u}_t$ and $\boldsymbol{\vartheta}$ must greater than zero, i.e.,

$$\|\boldsymbol{u}_t\| = \|\boldsymbol{\vartheta}\| > 0,$$

which can be achieved by guaranteeing the following condition

$$g - \ddot{\boldsymbol{p}}_d^T \boldsymbol{e_3} \neq 0.$$

Appendix B: Proof of Lemma 2

By using the definition of $[\boldsymbol{\omega}\times] = \boldsymbol{R}^T\dot{\boldsymbol{R}}$ and taking the time derivative of Eq. 28, the following holds

$$\boldsymbol{R_1}[\boldsymbol{\omega}_1\times]\boldsymbol{e_3} = \frac{d}{dt}\left(\frac{\boldsymbol{u}_t}{\|\boldsymbol{u}_t\|}\right) \equiv$$
$$\boldsymbol{\omega_1} = \begin{bmatrix} -\boldsymbol{W}\boldsymbol{R}_1^T\frac{d}{dt}\left(\frac{\boldsymbol{u}_t}{\|\boldsymbol{u}_t\|}\right) \\ \omega_{13} \end{bmatrix},$$

where $\omega_{13} = -\boldsymbol{b}_1^T\dot{\boldsymbol{b}}_2$, since $\boldsymbol{R_1}[\boldsymbol{\omega}_1\times]\boldsymbol{e_2} = \frac{d}{dt}(\boldsymbol{b_2})$. The computation of $\boldsymbol{\omega}_2$ follows the same approach, i.e.,

$$\boldsymbol{R_1}[\boldsymbol{\omega}_2\times]\boldsymbol{e_3} = \frac{d}{dt}\left(\frac{\boldsymbol{\vartheta}}{\|\boldsymbol{\vartheta}\|}\right) \equiv$$
$$\boldsymbol{\omega_2} = \begin{bmatrix} -\boldsymbol{W}\boldsymbol{R}_2^T\frac{d}{dt}\left(\frac{\boldsymbol{\vartheta}}{\|\boldsymbol{\vartheta}\|}\right) \\ \omega_{23} \end{bmatrix},$$

where $\omega_{23} = -\boldsymbol{d_1}^T \dot{\boldsymbol{d}}_{\boldsymbol{2}}$, since $\boldsymbol{R_2}[\boldsymbol{\omega}_2\times]\boldsymbol{e_2} = \frac{d}{dt}(\boldsymbol{d_2})$. The expression for the desired angular acceleration $\dot{\boldsymbol{\omega}}_1$ and $\dot{\boldsymbol{\omega}}_2$ follows directly from derivative in order to time of $\boldsymbol{\omega}_1$ and $\boldsymbol{\omega}_2$, respectively.

Then, by taking the derivative of Eq. 34, one can verify that

$$\boldsymbol{\omega}_d = \boldsymbol{R}_1^T(\boldsymbol{\omega}_2 - \boldsymbol{\omega}_1).$$

The expression for the angular acceleration $\dot{\boldsymbol{\omega}}_d$ is computed by taking the time derivative of $\boldsymbol{\omega}_d$.

By Assumption 1 and backed by Theorem 2, the variables $\boldsymbol{\omega}$, $\dot{\boldsymbol{\omega}}$, $\boldsymbol{x}_1$, $\dot{\boldsymbol{x}}_1$, and $\ddot{\boldsymbol{x}}_1$ are bounded signals. Consequently, the first and second time derivatives of $\boldsymbol{u}_t$ are bounded functions as well. Furthermore, from the assumptions on the references $\boldsymbol{p}_d$ and ψ_d given in Section 2.2 and by considering that Eq. 32 holds true, one may conclude, by inspection of $\boldsymbol{\omega}_d$ and $\dot{\boldsymbol{\omega}}_d$, that

$$|\boldsymbol{\omega}_d| \leq \Omega_1 \; \forall\, t \geq 0, \;\; \Omega_1 \in \mathbb{R}_{\geq 0}$$

$$|\dot{\boldsymbol{\omega}}_d| \leq \Omega_2 \; \forall\, t \geq 0, \;\; \Omega_2 \in \mathbb{R}_{\geq 0}.$$

Acknowledgements This work was supported by the Portuguese Fundação para a Ciência e a Tecnologia (FCT) through the scholarship 2020.06736.BD, and the Institute for Mechanical Engineering (IDMEC), under Associated Laboratory for Energy, Transports and Aeronautics (LAETA) [UID/EMS/50,022/2020] projects. This work has also been supported by the European Union under the Next Generation EU, through a grant of the Portuguese Republic's Recovery and Resilience Plan (PRR) Partnership Agreement, within the scope of the project PRODUTECH R3 - "Agenda Mobilizadora da Fileira das Tecnologias de Produção para a Reindustrialização", aiming the mobilization of the production technologies industry towards of the reindustrialization of the manufacturing industrial fabric (Project ref. nr. 60 - C645808870-00000067).

Author Contributions Author J. Madeiras contributed to designing, implementing the experiments, and writing the document. Authors C. Cardeira and P. Oliveira contributed to the analysis and interpretation of the results, development of the theoretical contributions, and composition of the manuscript.

Funding Open access funding provided by FCT|FCCN (b-on). This work was supported by the Portuguese Fundação para a Ciência e a Tecnologia (FCT) and the Institute for Mechanical Engineering (IDMEC).

Data Availability Authors can confirm that all relevant data are included in the article information files

Declarations

Conflicts of interest The authors declare that they have no conflict of interest.

Consent for publication Authors has consented to the submission to the journal.

Ethics approval Informed consent was obtained from all individual authors included in the study.

References

1. Idrissi, M., Salami, M.R., Annaz, F.: A review of quadrotor unmanned aerial vehicles: applications, architectural design and control algorithms. J Intell Robot Syst **104**, (2022)
2. Martins, L., Cardeira, C., Oliveira, P.: Linear quadratic regulator for trajectory tracking of a quadrotor. IFAC-PapersOnLine **52**(12), 176–181 (2019)
3. Martins, L., Cardeira, C., Oliveira, P.: Feedback linearization with zero dynamics stabilization for quadrotor control. J Intell Robot Syst **101**, (2021)
4. Moeini, A., Lynch, A.F., Zhao, Q.: Exponentially stable motion control for multirotor uavs with rotor drag and disturbance compensation. J Intell Robot Syst **103**(15), (2021)
5. D. Mellinger, V. Kumar, Minimum snap trajectory generation and control for quadrotors, In: 2011 IEEE International conference on robotics and automation, pp. 2520–2525 (2011)
6. T. Lee, M. Leok, N. H. McClamroch, Geometric tracking control of a quadrotor uav on se(3), In: 49th IEEE Conference on Decision and Control (CDC), pp. 5420–5425 (2010)
7. K. Gamagedara, M. Bisheban, E. Kaufman, T. Lee, Geometric controls of a quadrotor uav with decoupled yaw control. In: 2019 American Control Conference (ACC), pp. 3285–3290 (2019)
8. Invernizzi, D., Lovera, M., Zaccarian, L.: Integral iss-based cascade stabilization for vectored-thrust uavs. IEEE Control Syst. Lett. **4**(1), 43–48 (2020)
9. Mellinger, D., Michael, N., Kumar, V.: Trajectory Generation and Control for Precise Aggressive Maneuvers with Quadrotors, pp. 361–373. Springer, Berlin Heidelberg, (2014)
10. Control of vtol vehicles with thrust-tilting augmentation: IFAC Proceedings Volumes **47**(3), 2237–2244 (2014). 19th IFAC World Congress
11. Naldi, R., Furci, M., Sanfelice, R.G., Marconi, L.: Robust global trajectory tracking for underactuated vtol aerial vehicles using inner-outer loop control paradigms. IEEE Trans. Autom. Control **62**(1), 97–112 (2017)
12. Cabecinhas, D., Cunha, R., Silvestre, C.: A nonlinear quadrotor trajectory tracking controller with disturbance rejection. Control Eng. Pract. **26**, 1–10 (2014)
13. Yu, G., Cabecinhas, D., Cunha, R., Silvestre, C.: Quadrotor trajectory generation and tracking for aggressive maneuvers with attitude constraints. IFAC-PapersOnLine **52**(12), 55–60 (2019)
14. Xie, W., Yu, G., Cabecinhas, D., Cunha, R., Silvestre, C.: Global saturated tracking control of a quadcopter with experimental validation. IEEE Control Syst Lett **5**(1), 169–174 (2021)

15. Batista, P., Silvestre, C., Oliveira, P.: Optimal position and velocity navigation filters for autonomous vehicles. Automatica **46**(4), 767–774 (2010)
16. Cao, N., Lynch, A.F.: Inner-outer loop control for quadrotor uavs with input and state constraints. IEEE Trans Control Syst Technol **24**(5), 1797–1804 (2016)
17. G. Allibert, D. Abeywardena, M. Bangura, R. Mahony, Estimating body-fixed frame velocity and attitude from inertial measurements for a quadrotor vehicle, 2014 IEEE conference on control applications, CCA 2014 (2014)
18. Casau, P., Cunha, R., Silvestre, C.: Improved maneuverability for multirotor aerial vehicles using globally stabilizing feedbacks, pp. 3822–3827 (2020)
19. Lewis, F.L., Vrabie, D., Syrmos, V.L.: Optimal Control, 3rd edn., pp. 110–167. John Wiley & Sons, Ltd (2012)
20. Brockett, R.W.: Finite dimensional linear systems. Wiley (1970)
21. Khalil, H.K.: Nonlinear systems, 3rd edn. Prentice-Hall, Upper Saddle River, NJ (2002)
22. Zou, Y.: Nonlinear hierarchical control for quad-rotors with rotation matrix. Int J Control **90**(7), 1308–1318 (2017)
23. Invernizzi, D., Lovera, M., Zaccarian, L.: Integral iss-based cascade stabilization for vectored-thrust uavs. IEEE Control Syst Lett **4**(1), 43–48 (2020)
24. Naldi, R., Furci, M., Sanfelice, R.G., Marconi, L.: Robust global trajectory tracking for underactuated vtol aerial vehicles using inner-outer loop control paradigms. IEEE Trans Autom Control **62**(1), 97–112 (2017)
25. Mayhew, C.G., Sanfelice, R.G., Teel, A.R.: On path-lifting mechanisms and unwinding in quaternion-based attitude control. IEEE Trans. Autom. Control **58**(5), 1179–1191 (2013)
26. Bhat, S., Bernstein, D.: A topological obstruction to global asymptotic stabilization of rotational motion and the unwinding phenomenon. In: Proceedings of the 1998 American Control Conference. ACC (IEEE Cat. No.98CH36207), vol. 5, pp. 2785–2789 (1998)
27. Isidori, A., Marconi, L., Serrani, A.: Robust Autonomous Guidance An Internal Model Approach, 1st edn. Springer (2023)
28. Bani Younes, A., Mortari, D.: Derivation of all attitude error governing equations for attitude filtering and control. Sensors **19**, (2019)
29. Xie, W., Cabecinhas, D., Cunha, R., Silvestre, C.: Adaptive backstepping control of a quadcopter with uncertain vehicle mass, moment of inertia, and disturbances. IEEE Trans. Ind. Electron. **69**(1), 549–559 (2022)
30. Lee, D.: Ar. drone 2.0 support from embedded coder, (2016). https://github.com/darenlee/SimulinkARDroneTarget
31. Jeurgens, N.:Identification and control implementation of an ar.drone 2.0, Master's thesis, Eindhoven University of Technology (2017)
32. Yu, G., Cabecinhas, D., Cunha, R., Silvestre, C.: Nonlinear backstepping control of a quadrotor-slung load system. IEEE/ASME Trans. Mechatron. **24**(5), 2304–2315 (2019)

João Madeiras is a Ph.D. student from the Instituto Superior Técnico (IST), Lisbon, Portugal. He completed his master's degree in mechanical engineering with a thesis on Estimation Methods for position and attitude with Quadrotors. He received three diplomas for academic excellence and one for academic merit during his studies. He has been with the Mechanical Engineering Institute, IST, where he is currently pursuing his PhD in Inspection with Unmanned Aerial Vehicles. His research interests include nonlinear observers and controllers, inertial navigation systems, and vision systems, with application to autonomous vehicles.

Carlos Cardeira was born in Quinjenje, Angola, and received the engineering and master of science degrees in 1986 and 1991, in electrical engineering from Instituto Superior Técnico in Lisbon – Portugal. In 1994 he received the PhD in electrical engineering and computer science from the Institut National Polytechnique de Lorraine in Nancy – France. He is a member of the Center of Intelligent Systems of the IDMEC research laboratory and teaches at Instituto Superior Técnico in Lisbon courses in Mechatronics Systems, Industrial Automation and Informatics areas. He made several post-docs and sabbatical leaves, namely in IRIT and LAAS in Toulouse-France, CERN in Geneva – Switzerland and Schneider-Electric in Seligenstadt-Germany.

Paulo Oliveira (Hab 16 Ph.D.'02 M.Sc.'91) received the "Licenciatura", M.S., and Ph.D. degrees in Electrical and Computer Engineering, and the Habilitation in Mechanical Engineering from Instituto Superior Técnico (IST), Lisbon, Portugal, in 1991, 2002, and 2016, respectively. He is an Associate Professor in the Department of Mechanical Engineering of IST and Senior Researcher in the Associated Laboratory for Energy, Transports, and Aeronautics. His research interests are in the area of autonomous robotic vehicles with a focus on the fields of estimation, sensor fusion, navigation, positioning, and mechatronics. He is author or coauthor of more than 80 journal papers and 175 conference communications. He participated in more than 30 European and Portuguese research projects, over the last 30 years.